Author Manuscript

Title: Perovskite Oxide-Based Electrodes for High-Performance Photoelectrochemical Water Splitting: A Review

Authors: Wei Wang; Meigui Xu; Xiaomin Xu; Wei Zhou; Zongping Shao, Ph.D

To be cited as: 10.1002/anie.201900292

Link to VoR: https://doi.org/10.1002/anie.201900292

Perovskite Oxide-Based Electrodes for High-Performance Photoelectrochemical Water Splitting: A Review

Wei Wang,[+[a]] Meigui Xu,[+[a]] Xiaomin Xu,[[b]] Wei Zhou,[[a]] and Zongping Shao*[[a, b]]

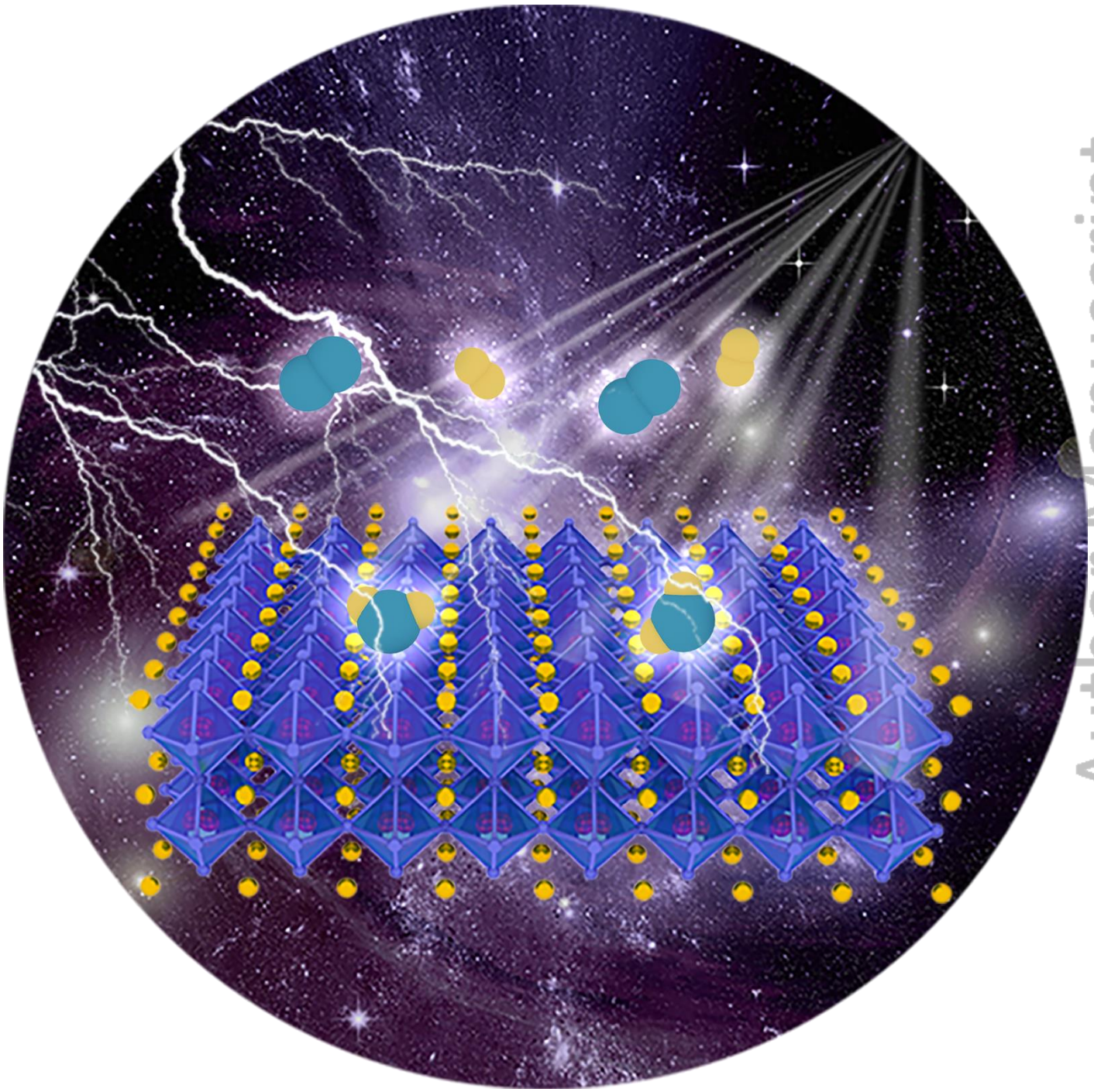

Abstract: Photoelectrochemical (PEC) water splitting is an attractive strategy for the large-scale production of renewable hydrogen from water. Developing cost-effective, active and stable semiconducting photoelectrodes is extremely important for achieving PEC water splitting with high solar-to-hydrogen efficiency. Perovskite oxides as a large family of semiconducting metal oxides are extensively investigated as electrodes in PEC water splitting owing to their abundance, high (photo)electrochemical stability, compositional and structural flexibility allowing the achievement of high electrocatalytic activity, superior sunlight absorption capability and precise control and tuning of band gaps and band edges. In this review, the research progress in the design, development, and application of perovskite oxides in PEC water splitting is summarized, with a special emphasis placed on understanding the relationship between the composition/structure and (photo)electrochemical activity.

1. Introduction

Nowadays, research scientists are seeking renewable and clean energy sources to replace non-renewable fossil fuels to meet the requirement of energy supplies and address the relevant environmental concerns. Hydrogen gas (H_2), with higher gravimetric energy density than gasoline (120 vs. 44 MJ kg^{-1}), no carbon emission, and renewable and storable nature is considered as an advanced energy carrier to substitute traditional fossil fuels.[1] Nowadays, H_2 can be produced directly through several routes such as steam reforming/partial oxidation of hydrocarbons, coal gasification, and water splitting, etc.[2-5] Among these technologies, water splitting has attracted rapidly increasing attention due to the high abundance of water (covering ~71% of the Earth's surface), the high purity of H_2 as generated through water splitting, no requirement of high temperature, and great reduction in CO_2 emissions.[6-9]

Among the various water splitting systems, solar energy-based water splitting devices have attracted growing attention due to the fact that solar energy is considered as the most abundant energy source since approximately 36,000 TW of the solar energy can reach the land each year. More specifically, if 0.1% of the sunlight energy reaching the Earth per year can be effectively utilized, it is sufficient to meet the predicted annual energy consumption amount in 2050.[10] Water splitting using solar energy can be categorized into four main classes including photocatalytic water splitting, solar-cell-powered electrochemical water splitting, solar thermochemical water splitting, and photoelectrochemical (PEC) water splitting.[11-19]

[a] Prof. W. Wang[+], M. Xu[+], Prof. W. Zhou, Prof. Z. Shao
State Key Laboratory of Materials-Oriented Chemical Engineering, College of Chemical Engineering
Nanjing Tech University
Nanjing, 210009, P. R. China
E-mail: shaozp@njtech.edu.cn
[b] X. Xu, Prof. Z. Shao
WA School of Mines: Minerals, Energy and Chemical Engineering (WASM-MECE)
Curtin University
Perth, WA 6845, Australia
[+] These authors contributed equally to this work.

Wei Wang obtained his PhD degree in chemical engineering at Nanjing Tech University, China, in 2013. He then worked as a postodc at Curtin University, Australia and was promoted to research fellow in 2015. In 2018, he became a professor at Nanjing Tech University. His research interests include the developement of advanced electrodes and fuels for solid oxide fuel cells and the design of perovskites for photocatalysis- and photovoltaics-related energy conversion and environmental treatment.

Zongping Shao is a professor of chemical engineering at Nanjing Tech University, China and Curtin University, Australia. He obtained his PhD from Dalian Institute of Chemical Physics, China in 2000. He worked as a visiting scholar at Institut de Researches Sur La Catalyse, CNRS, France and postdoc at California Institute of Technology, USA from 2000 till 2005. His current research interests include solid-oxide fuel cells, lithium-ion batteries, oxygen-permeable membranes and low-temperature energy-conversion devices.

In solar electrolysis, solar cells are widely applied to provide the electricity needed for the electrolysis. The ease with which the solar cell-electrolysis cell (SC-EC) system can be scaled up represents an advantage for industrial applications. This superiority of SC-EC system is realized by the integration of two matured infrastructures, i.e., a high-performance solar cell as the electricity supplier and an electrolysis cell for H_2 production. However, unlike the direct sunlight harvesting in PEC water splitting, the two-step SC-EC system could add to an inevitable efficiency loss.[20] Furthermore, electrochemical water splitting occurs only at a considerable voltage associated with the large overpotentials needed to drive the kinetically sluggish water oxidation and reduction half reactions, leading to significant energy losses even facilitated by state-of-the-art noble metal-based electrocatalysts (not to mention the prohibitive cost of these catalysts).[21] Photocatalytic water splitting is an advanced technology to utilize solar energy to produce H_2, which shows several merits such as low cost, size flexibility, and relatively high solar-to-hydrogen (STH) efficiency. In the solar thermochemical water splitting route, concentrated solar radiation is used as the energy source to provide high-temperature process heat in order to drive the endothermic water splitting. Advantages of this route in generating H_2 include low electrical energy requirement, no membranes needed to

separate H_2 and O_2, and all principally recycled chemicals used in this route.

The PEC water splitting process is considered to be one of the most promising options to reorganize electrons in H_2O to convert solar energy to chemical energy stored in H_2. In PEC water splitting, the overpotential for water oxidation/reduction is compensated by applying a bias in part.[22] Accordingly, the oxidation of water (i.e., oxygen evolution reaction, OER) or the reduction of water (i.e., hydrogen evolution reaction, HER) in PEC water splitting could be achieved at potentials lower than 1.23 V vs. reversible hydrogen electrode (RHE) or higher than 0 V vs. RHE, respectively, which are the equilibrium potentials of the two half reactions at room temperature. PEC water splitting is superior to solar cell-powered electrochemical water splitting, photocatalytic water splitting and solar thermochemical water splitting due to several reasons as illustrated below. Firstly, a low overpotential is required to drive the PEC water splitting, suggesting a superior STH efficiency, while several photovoltaic devices (solar cells) are needed in series to provide the potential required in electrocatalytic water splitting (~2.0 V).[16,17] Secondly, simultaneously high activity of the photocatalyst for OER and HER cannot be easily obtained in photocatalytic water splitting while high OER and HER activity can be achieved by rationally selecting the photocathodes and photoanodes in PEC water splitting.[23] Thirdly, pure H_2 and O_2 can be easily separated and obtained through PEC water splitting while the environmentally benign separation of O_2 from explosive H_2 and O_2 mixtures is a critical issue in photocatalytic water splitting.[23] Fourthly, high process temperature and multiple steps are not needed in PEC water splitting as compared with the solar thermochemical water splitting.

The development and design of active and durable PEC water splitting systems have attracted sharply increased attention in the past decade.[24-28] In particular, photoelectrodes are the core part of the PEC water splitting devices, which harvest sunlight to produce electron-hole pairs with subsequent separation and transportation processes. Metal oxides, sulfides, and nitrides are promising photoelectrodes in PEC water splitting,[29-34] among which metal oxides including TiO_2, ZnO, SnO_2, Fe_2O_3, and WO_3 are predominantly explored due to their low cost, suitable semiconducting properties, superior stability, abundance and easy nanostructuring capability.[35-40] According to the working principles of PEC water splitting, photoelectrodes, especially the photoanode, should have both high electrocatalytic activity and sunlight absorption capability to achieve high STH efficiency, which cannot be easily obtained by simple metal oxides due to the fixed atomic environment. Based on this consideration, perovskite oxides (ABO_3) are more attractive than simple oxides as photoelectrodes in PEC water splitting, which is due to their high activity/durability and excellent compositional and structural flexibility, holding the possibilities to achieve high electrocatalytic activity, superior sunlight absorption capability and precise control of band gaps and band edges simultaneously. More specifically, alkali metals (Li, Na, etc.), alkaline-earth metals (Ba, Sr, etc.) and rare-earth metals (La, Pr, etc.) can occupy the A site of perovskite oxides while a number of transition metals (Ti, Fe, Co, Mn, Ta, etc.) can be used as the B-site elements.[23,41,42] In addition, both A and B sites can be substituted by other metal cations to form $A_{1-x}A'_xBO_3$ or $AB_{1-y}B'_yO_3$. Furthermore, the adjustable bulk and surface components as well as the easy tailoring of the physical and chemical properties of perovskite oxides offer great potential to tune the photoexcitation and water activation processes in PEC water splitting, which may enhance the (photo)electrochemical activity and STH efficiency.

Given that the OER at the anode is the rate-determining step in water splitting, the development of highly active photoanodes for OER has captured extensive attention. Some studies focused on TiO_2 photoanodes for PEC water oxidation.[43-45] Nevertheless, due to a large band gap (~3.2 eV), TiO_2 can only harvest sunlight in the ultraviolet (UV) region. As the UV light only constitutes 4% of the solar energy, the theoretical STH efficiency of TiO_2 photoanodes can only reach ~2% under solar irradiation, even when assuming 100% absorbed-photon-to-hydrogen conversion efficiency.[43-45] It is therefore necessary to develop semiconductors with sunlight absorption capability in the visible light region that constitutes ~45% of the solar energy. Due to the structural flexibility of perovskite oxides, the oxygen in perovskite oxides can also be partially substituted by non-metal elements (e.g., Cl, N, S, etc.) to suppress the band gap and improve the visible light absorption capability.[46-49] Additionally, the rational selection and functional doping of A-site elements in perovskite oxides can also lead to the reduction of band gaps.[50-52]

It is intriguing to mention that for some perovskite-based photoelectrodes with visible light response, they can also function as promising electrocatalysts for water splitting reactions. For instance, $LaFeO_3$, a popular photoelectrode in PEC water splitting, has been demonstrated to catalyze the electrocatalytic OER, showing potential for improved electrocatalysis when A-site La-deficiency is further introduced.[53] Another example is oxygen-deficient nanosized $BaTiO_{3-\delta}$, which exhibits high electrocatalytic activity for OER, outperforming the OER activity of noble-metal-based IrO_2 at relatively low overpotentials.[54]

The rapid progress in the design of cost-effective electrocatalysts for PEC water spitting has motivated the researchers to give a comprehensive summary of advances in this emerging and dynamic field. Up to now, several review articles on PEC water spitting are available in open literature, focusing on the system design, material development, selected promising materials, nanostructuring and kinetics aspects.[55-61] However, there is still no review about the application, design, and development of the specific category of perovskite oxides in PEC water splitting. This paper aims to summarize research advances in the design and development of perovskite oxides for PEC water splitting with a particular emphasis on structural design, defect control, band gap engineering, interface/nanostructure construction and heterojunction/morphology control. The strategies for improving the PEC performance of perovskite oxides are highlighted. In the end, the challenges and future directions about the research of perovskite oxide-based electrodes for PEC water splitting are provided.

2. Principles of PEC Water Splitting and Selection Criteria for Photoelectrodes

2.1. Principles of PEC Water Splitting

The PEC water splitting reaction is an endothermic process and the energy needed to drive this reaction is provided by the sunlight and bias. Figure 1a displays a graphic representation of the one-step photocatalytic water splitting.[55] The electrons in the valence band (VB) of a semiconductor are photoexcited to the conduction band (CB) when the semiconductor absorbs solar energy larger than its band gap energy. Thus, the holes are produced in the VB. The photoexcited and separated electrons/holes migrate to the catalyst surface and subsequently participate in the redox reactions. To realize the photocatalytic water splitting based on one photocatalyst, the band gap of the semiconducting photocatalyst should sandwich between the potentials of water reduction and oxidation reactions as shown in Figure 1a, which is demonstrated as the working principle of one-step water splitting. In addition to the one-step water splitting, two semiconductors can be coupled in series with the help of redox couples (Figure 1b), which is named as two-step water spitting reaction ("Z-scheme" water splitting). In this two-step water spitting, the water reduction and the oxidation of redox couples happen on one photocatalyst while the water oxidation and the reduction of redox couples occur on the other photocatalyst.[62]

For PEC water splitting, in the n-type semiconducting photoanodes, the photoinduced holes accumulate on the semiconductor surface and then participate in the oxidation reactions (Figure 1c). On the other hand, the electrons migrate to a counter electrode (CE) via an external circuit and participate in the reduction reactions (Figure 1c). The top of the VB of the semiconductor-based photoanode should be more positive than the potential for the OER while the CB edge of the semiconductor-based photocathode should be more negative than the potential for the HER (Figure 1d). In PEC water splitting, an external bias is used to compensate the potential gap between the potential of electrons on the CE and the Fermi level of the photo-excited photoelectrode to drive the redox reactions on the photoelectrode surfaces. On the other hand, a photoanode and a photocathode can be coupled in series instead of using a single photoelectrode and a CE (Figure 1e), which is similar to that of the Z-scheme water splitting.[63]

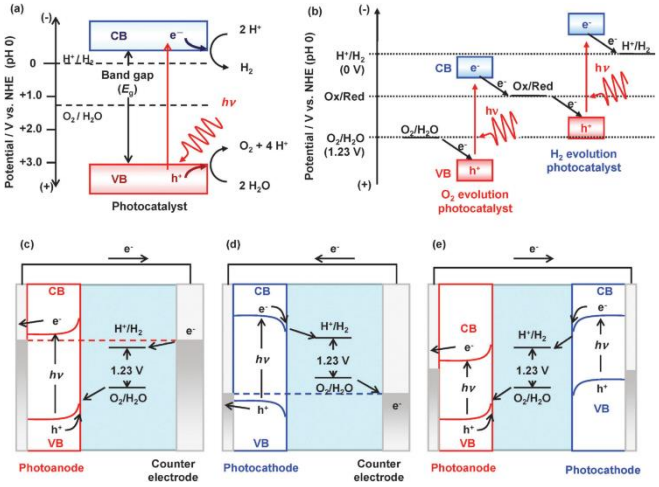

Figure 1. Energy diagrams of (a) one-step and (b) two-step photocatalytic water splitting, and PEC water splitting using (c) a photoanode, (d) a photocathode, and (e) both photoanode and photocathode in a tandem configuration. Reproduced with permission from ref. [55], Copyright 2014, Royal Society of Chemistry.

Under sunlight illumination, the electrons in the semiconducting photoelectrodes are activated from the VB to the CB. As a result, some of the generated electrons migrate to photocathode surface to reduce water, whereas some holes transfer to the photoanode surface to oxidize water, although most of the photoinduced electrons and holes quench inevitably. These two half-reactions in PEC water splitting, namely HER and OER, contribute quite significantly to the overall STH efficiency. In addition to the photochemical pathways (photoinduced charge carrier production, separation and transportation) in the bulk of the semiconducting electrodes, cocatalysts are also key components for PEC water splitting because they can promote the photoinduced charge carrier separation/transportation and function as the active sites to catalyze the HER/OER (Figure 2a-c). Furthermore, the use of cocatalysts may reduce the possibility of photocorrosion and enhance the chemical stability of semiconductor-based photoelectrodes.

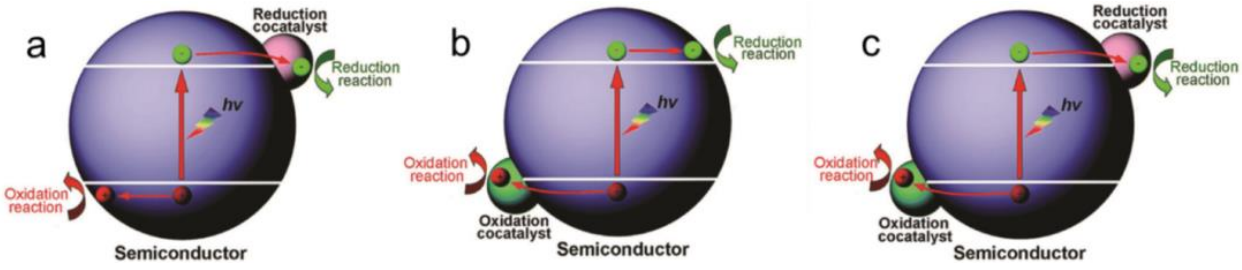

Figure 2. Schematic representations of semiconductors with cocatalysts on the surface in different configurations. (a) Semiconductor/HER cocatalyst configuration, (b) semiconductor/OER cocatalyst configuration, and (c) HER cocatalyst/semiconductor/OER cocatalyst configuration. Reproduced with permission from ref. [57], Copyright 2017, Wiley-VCH.

2.2. Selection Criteria for Photoelectrodes/Cocatalysts and the Superiority of Perovskite Oxides

Based on the working principles of PEC water splitting mentioned above, an active photoelectrode material should meet the prerequisites as shown below. First of all, the photoelectrodes must absorb sunlight with energy larger than 1.23 eV, which enables efficient PEC water splitting by overcoming the overpotential in the HER and OER. The photoelectrodes should also possess superior sunlight absorption capability to produce enough photoinduced charge carriers. Thus, semiconductors with large band gap and low visible light response are not favorable although they may have proper band edge positions for water splitting reactions. Secondly, fast charge separation/transfer in semiconductors is also essential to achieve high PEC performance. Efficient separation of electron-hole pairs can suppress the potential recombination loss and increase the number of charge carriers available for the surface reactions in PEC water splitting. Thirdly, the semiconducting photoelectrodes should display high electrocatalytic activity for the HER and OER half reactions.

Among the widely used semiconducting photoelectrodes in PEC water splitting, metal oxides have attracted increasing attention because of the low cost, superior chemical and anti-photocorrosion stability, as well as proper band edge positions.[42] However, metal oxides have their own intrinsic limitations or drawbacks. For example, ZnO and TiO_2 with large band gaps (~3.2 eV) show almost no visible light absorption capability, while Fe_2O_3 displays proper band gap with visible light response (2.2 eV) but is limited by low transport and extraction rates of the photoinduced charge carriers which is associated with the sluggish polaron hopping rate and low electrical conductivity.[59] The low electrical conductivity of simple oxides also leads to significantly increased energy consumption amount and an obvious internal potential loss, which may have a negative effect on the PEC performance. The structural and compositional flexibility of perovskite oxides may meet the above-mentioned three main prerequisites for the electrodes/cocatalysts in PEC water splitting such as 1) suitable band gap with visible light response, 2) charge transfer/separation capability and 3) high electrocatalytic activity for HER and OER half reactions.

2.2.1. **Band Gap Engineering**

By tailoring the A-site, B-site and O-site elements in perovskite oxides, their band gaps can be reduced to 1.7-2.4 eV, showing different colors with various visible light responses.[42] The band gaps of perovskite oxides were optimized by rationally selecting the A-site and B-site cations and O-site anions. A-site Zn doping was demonstrated to reduce the band gap energy of $BaTiO_3$ and $SrTiO_3$.[64] Zou et al. demonstrated that the Zn doping suppressed the band gap of $BaTiO_3$ and $SrTiO_3$. With increasing the Zn doping amounts, the band gap values decreased due to the increased contribution of the Zn-3d orbital to the CBs of the perovskite oxides.[64] For the B-site doping, Hwang et al. investigated the effect of B-site metal dopants on the band gap and visible light response of the layered $La_2Ti_2O_7$ perovskite and found that Cr and Fe-doped $La_2Ti_2O_7$ displayed visible light absorption due to the decreased band gap.[65] In addition, these two catalysts showed considerable photocatalytic activity for water splitting reaction to produce H_2 under visible light illumination.[65] Nitrogen (N) doping in the O site of perovskite oxides was demonstrated as another effective strategy to suppress the band gap.[42] A considerable reduction in band gap (from ~4.06 to ~1.76 eV) was obtained by doping N into the $Ba_5Ta_4O_{15}$ perovskite.[66] The N-doped $Ba_5Ta_4O_{15}$ displayed an obviously enhanced photocatalytic activity for HER (~50%) as compared to $Ba_5Ta_4O_{15}$ under simulated sunlight illumination.

2.2.2. **Charge Transfer/Separation Capability**

The intrinsic conductivity of perovskite oxides can be greatly enhanced through the rational selection of A/B site elements and B-site doping with non-metal elements such as phosphorus (P) and boron (B).[67-71] For example, $NdBa_{0.25}Sr_{0.75}Co_2O_{5.9}$ and $NdBa_{0.25}Sr_{0.75}Co_2O_{5.93}$ possess high electrical conductivities of 5400 and 6200 $S\,cm^{-1}$ at room temperature, respectively.[72] Lee et al. studied the conductivity dependency of the activity of perovskite oxides for electrocatalytic oxygen reduction reaction and found that high electrical conductivity of the catalysts (e.g., $NdBa_{0.25}Sr_{0.75}Co_2O_{5.9}$ and $NdBa_{0.25}Sr_{0.75}Co_2O_{5.93}$) is critical for the achievement of high electrocatalytic activity by providing the internal conducting pathways.[72] The P-doped $SrCoO_{3-\delta}$ ($SrCo_{0.95}P_{0.05}O_{3-\delta}$) displayed >100 times enhancement in the electrical conductivity as compared with $SrCoO_{3-\delta}$, leading to an enhanced OER activity.[71] The above results suggest that the electrocatalytic performance can be greatly enhanced by increasing the electrical conductivity through rational selection of the compositional elements and functional dopants as well as control of the oxygen vacancy concentration in perovskite oxides.

2.2.3. **High Electrocatalytic Activity for HER and OER**

Nowadays, precious metals are the most active co-catalysts to promote the electrocatalytic activity of most metal oxide-based photoelectrodes in the PEC water splitting.[73] For instance, Pt shows the highest HER activity while IrO_2 and RuO_2 are the most efficient electrocatalysts for the OER.[74-76] However, these electrocatalysts all suffer from low abundance, high price and limited bifunctionality that hinder their large-scale practical applications. Some perovskite oxides such as $Pr_{0.5}Ba_{0.25}Sr_{0.25}Co_{0.8}Fe_{0.2}O_{3-\delta}$, $SrCo_{0.9}Ir_{0.1}O_{3-\delta}$ and $NdBaMn_2O_{5.5}$ are demonstrated as highly efficient electrocatalysts for water splitting in alkaline or acidic electrolytes, showing superior OER activity to that of IrO_2/RuO_2 and comparable HER activity to that of Pt.[77-82] More specifically, $Pr_{0.5}Ba_{0.25}Sr_{0.25}Co_{0.8}Fe_{0.2}O_{3-\delta}$ perovskite is one of the pioneering electrocatalysts for HER in alkaline solution and comparable HER activity as well as superior durability to those of Pt were achieved.[77] Perovskite oxides with visible light response such as $LaFeO_3$, doped $LaFeO_3$, Fe doped $SrTiO_3$ are demonstrated to show

considerable electrocatalytic activity for the HER and OER, which may have the possibilities to function as photoelectrodes and cocatalysts simultaneously.[53,54,83-88]

Due to the large kinetic barriers of OER in water splitting, researchers mainly focus on the development of high-performance OER electrocatalysts based on visible-light-active $LaFeO_3$ perovskite oxide through A-site doping, B-site doping and the tuning of the cation deficiency.[53,86,87] For example, A-site Sr-doped $LaFeO_3$ perovskite oxides with various compositions of $La_{1-x}Sr_xFeO_{3-\delta}$ (x= 0, 0.2, 0.5, 0.8 and 1) were developed as electrocatalysts for the OER.[87] It was found that Sr doping enhanced the OER activity and $La_{0.2}Sr_{0.8}FeO_{3-\delta}$ showed the highest OER activity in terms of overpotential, onset potential and Tafel slope among the five perovskite oxides due to the optimized oxygen vacancy concentration and B-site metal valence state on the catalyst surface. More specifically, with the increase in the Sr doping amount in the perovskite, the oxygen vacancy concentration increased in the order of $LaFeO_3$< $La_{0.8}Sr_{0.2}FeO_{3-\delta}$ < $La_{0.5}Sr_{0.5}FeO_{3-\delta}$ < $SrFeO_{3-\delta}$ < $La_{0.2}Sr_{0.8}FeO_{3-\delta}$. The relative amount of Fe^{4+} increased with increasing Sr content, following the order of $LaFeO_3$ < $La_{0.8}Sr_{0.2}FeO_{3-\delta}$ < $La_{0.5}Sr_{0.5}FeO_{3-\delta}$ < $La_{0.2}Sr_{0.8}FeO_{3-\delta}$ < $SrFeO_{3-\delta}$. Due to the strong binding energy of Fe^{4+} to the reaction intermediate species (*OH) in the OER, excessive Fe^{4+} can hinder the detachment of OH^- and subsequent oxygen gas release. As a result, $La_{0.2}Sr_{0.8}FeO_{3-\delta}$ with appropriate binding strength for reaction intermediates to the perovskite surface and the highest oxygen vacancy concentration displayed the best OER activity. B-site P-doped $LaFeO_3$ was demonstrated as an OER electrocatalyst in an alkaline solution due to the increased amount of O_2^{2-}/O^- species, the formation of Fe^{4+} species, the optimized e_g electron filling (≈ 1), and the enhanced adsorption capability of O_2 and hydroxyl groups on the surface originating from the P doping in the B-site of $LaFeO_3$.[86] Besides the A-site and B-sited doped perovskites as electrocatalysts for the OER, Zhu et al. developed a useful strategy for enhancing OER activity of $LaFeO_3$ in alkaline solutions by introducing A-site cation deficiency.[53] Among the investigated A-site cation deficient perovskite oxides, $La_{0.95}FeO_{3-\delta}$ showed the best activity for OER, which was assigned to the formation of oxygen vacancies and active Fe^{4+} species.

Very recently, Sr-doped $LaFeO_3$ was used as a photoanode for PEC water oxidation without the addition of cocatalysts, showing considerable OER activity.[89] The Sr doping in $LaFeO_3$ with a proper doping concentration promoted the oxidation of iron ions and then reduced the band gap. As a result, the onset potential and overpotential for the OER was obviously reduced at the expense of photocurrent density when 12 mol.% of Sr was doped into the $LaFeO_3$ perovskite.

3. Recent Advances in Perovskite Oxides as Electrodes for PEC Water Splitting

3.1. Bulk Composition Tailoring

Although most of the reported STH efficiencies in PEC water splitting are very low up to now, STH efficiency as high as 30% can be obtained in principle when a semiconductor-based light absorber shows a band gap of 1.6 eV. Thus, the engineering of the band gaps of semiconductor-based electrodes is critical, which can be easily realized by functional doping in metal oxides.[23] In addition, the optical, electrical, and physical features of metal oxides can be enhanced by adding extrinsic impurities or creating intrinsic defects through doping. The doping in metal oxides can also bring about some impurity energy states to reduce the band gap and to modify the electronic properties.[23,59] Typically, the PEC activity of TiO_2 was improved by the creation of oxygen vacancies through a hydrogen treatment, which functioned as the electron donors.[90] However, the dopants in such doped metal oxide-based photocatalysts serve not only as visible-light capture centers, but also as recombination sites for the photoinduced electron-hole pairs. Thus, the selection of dopants as well as the doping amount should be tailored carefully to achieve an optimized PEC performance.

The selective and functional doping in the B and O sites of perovskite oxides is the most used strategy to reduce the band gap to obtain high PEC performance under visible light irradiation.[91-96] For instance, Fe doping was used to suppress the band gap of $BaTiO_3$ nanopowder and to improve the PEC performance.[97] $BaTiO_3$ perovskite oxides with various Fe doping amounts of 0.5-4.0 at.% were prepared by a polymeric precursor method. The Fe doping suppressed the band gap of $BaTiO_3$ from 3.11 to 2.81 eV, and then an enhanced PEC activity under visible light illumination was achieved. The origin of the improved PEC performance of Fe-doped $BaTiO_3$ was studied by calculating the electronic structure and state associated with Fe doping.[97] The Fe doping in $BaTiO_3$ increased the electrical conductivity and decreased the amount of recombination centers, which led to an improvement in the photocarriers' lifetime and the photoconductivity. Doping of $BaTiO_3$ with an optimal Fe doping level of 2.0 at.% resulted in an obvious enhancement in the photocurrent density compared to undoped $BaTiO_3$ (2.55 vs. 0.07 mA cm^{-2}).

Non-metal element doping, particularly N doping, has been reported to be useful to enhance the PEC performance of perovskite oxides under visible light.[98-103] Nb-based perovskite oxynitrides such as $BaNbO_2N$ and $SrNbO_2N$ were prepared from stoichiometric $BaNbO_3$ and $SrNbO_3$ by a thermal ammonolysis route, which showed sunlight harvesting capability at 700 nm (for $SrNbO_2N$) and even higher than 700 nm (for $BaNbO_2N$).[104] The preparation of $BaNbO_2N$ using cubic structured $BaNbO_3$ effectively improved the bulk and surface crystallinity of the perovskite oxynitride by avoiding structural transition during the nitridation process when compared to the use of $Ba_5Nb_4O_{15}$ as the precursor.[104] This method minimized the amount of surface anion defects, which contributed to a relatively high PEC-OER activity with a current density of 0.85 mA cm^{-2} at 1.23 V vs. RHE under simulated sunlight irradiation.

Several nitrogen-doped Nb-based perovskite oxides such as $CaNbO_2N$, $SrNbO_2N$, $BaNbO_2N$ and $LaNbON_2$ with similar band gaps were reported as photocatalysts for water splitting reaction under visible light irradiation.[105] Nevertheless, among these four photocatalysts, only $CaNbO_2N$ displayed a

considerable activity for HER and OER under visible light. The different photocatalytic activities of these N-doped perovskite oxides with comparable band gap were assigned to the differences in the band edge positions. Thus, it suggests that, besides the band gap energy, the absolute band energy positions of perovskite oxides should also be optimized to enhance the OER and HER performance in PEC water splitting. As a result, due to the intrinsic kinetic limitations of the OER and HER and the resulting overpotential needed for these two reactions, a band gap of around 2.0 eV is frequently reported as the threshold energy required to achieve a reasonable PEC activity. In this regard, $LaFeO_3$ with a band gap of around 2.0 eV has been investigated as the photoelectrode in PEC water splitting.[106-108] For example, $LaFeO_3$ with a band gap of 1.95 eV was prepared by a sol-gel method and the corresponding photoanode was formed by dip-coating and calcination.[108] The PEC performance studies suggested that $LaFeO_3$ photoanode showed a high photocurrent density of 8.2 mA cm^{-2} at 1.7 V vs. Ag/AgCl. However, $LaFeO_3$ still suffered from the extremely low PEC activity at a lower bias such as 1 V vs. Ag/AgCl. Thus, the functional doping of $LaFeO_3$ was demonstrated to enhance the PEC performance.[109]

The doping of transition metals such as Mn, Co, and Cu in $LaFeO_3$ was used to tailor the electrical and optical properties in order to enhance the PEC-OER activity under visible light illumination.[109] The doping effectively decreased the onset photo-potential of $LaFeO_3$ photoanode. As shown in Figure 3a, the onset photo-potentials were 0.48, 0.27, 0.34, and 0.27 V for $LaFeO_3$, $LaFe_{0.9}Cu_{0.1}O_3$, $LaFe_{0.9}Mn_{0.1}O_3$, and $LaFe_{0.9}Co_{0.1}O_3$, respectively. The photocurrent densities were 0.99, 0.85 and 0.52 mA cm^{-2} for Cu, Co and Mn doped $LaFeO_3$ at a bias of 1 V, respectively. As shown in Figure 3b, sensitive photocurrent responses were observed upon the switch from the dark condition to the sunlight, suggesting the fast photocurrent production. The photocurrent density of $LaFeO_3$ was 0.01 mA cm^{-2} and this value was enhanced to 0.21, 0.21 and 0.06 mA cm^{-2} for the Cu, Co and Mn doped samples, respectively. It was found that the 10% doping amount was the optimal amount to enhance the PEC activity of $LaFeO_3$ while excessive dopants may act as recombination sites, which reduced the transportation efficiency of electron-hole pairs to the surface. Figure 3c displays the photocurrent density of different doped $LaFeO_3$ with various doping levels. In all these doped samples, the highest photocurrent density was achieved at a doping concentration of 10% as compared with the samples with 5 and 20% doping concentrations. A photo-conversion efficiency (PCE) of 0.22% was observed on $LaFeO_3$ as shown in Figure 3d while this value was enhanced to 0.51, 0.31 and 0.37% for $LaFe_{0.9}Cu_{0.1}O_3$, $LaFe_{0.9}Mn_{0.1}O_3$ and $LaFe_{0.9}Co_{0.1}O_3$, respectively. The improved charge transfer capability and the increased carrier densities of the doped $LaFeO_3$ contributed to the enhanced PEC activity.

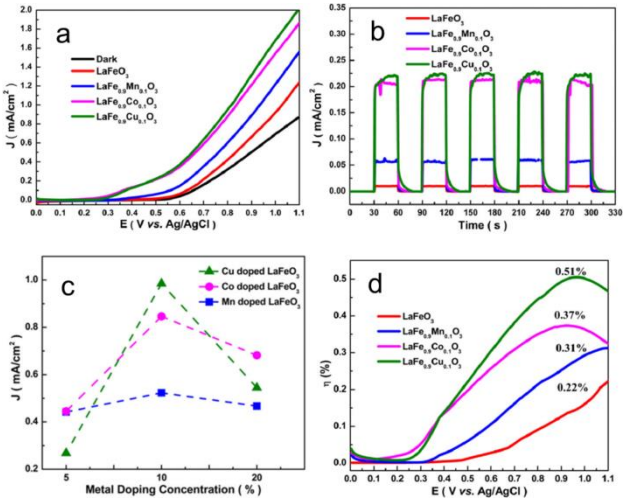

Figure 3. (a) Photocurrent density vs. voltage curves and (b) transient photocurrent response of pristine $LaFeO_3$ and doped $LaFeO_3$ samples, (c) Photocurrent density of Mn, Co, Cu doped $LaFeO_3$ with various doping amounts, (d) PCEs vs. voltage curves of pristine $LaFeO_3$ and doped $LaFeO_3$ samples. Reproduced with permission from ref. [109], Copyright 2015, Elsevier.

3.2. Nanostructure Construction and Morphology Control

Various approaches are applied to address the drawbacks of metal oxide-based photoelectrodes such as low surface areas and large particle sizes. Compared to the bulk counterparts, the nanostructured materials with reduced particle size and enlarged surface area reduce the diffusion length of photoinduced electron-hole pairs and promote their separation, and then improve the charge carrier collection and utilization efficiency. Thus, a much improved PEC activity can be obtained on nanostructured photoelectrodes. Nanostructured metal oxides with different morphologies (e.g., nanoparticles, nanotubes, nanoplatelets, etc.), including WO_3, ZnO, Fe_2O_3, TiO_2, Cu_2O, $BiVO_4$, $BiFeO_3$ and $SrTiO_3$, have been widely studied as electrodes for PEC water splitting.[28,39,110-115]

Lead magnesium titanate (PMT) perovskite oxides with four different morphologies such as nanospheres (PMTS), flakes (PMTF), hierarchical flower (PMTH) and thin microbelt (PMTT) were reported with scanning electron microscopy (SEM) images shown in Figure 4, which were rationally tailored by a solution-based method for the application as photoanodes in PEC water splitting.[116] The effect of solvent on the structure, crystallinity, morphology, sunlight absorption capability of PMT was systematically studied. Among the various photoanodes, PMTT showed the highest PEC activity and the corresponding PCE value was ~3.90, 3.54, 2.85 and 1.52 times larger than that of $PbTiO_3$, PMTS, PMTF and PMTH perovskite oxides, respectively. The excellent PEC water splitting performance of PMTT was assigned to the lager number of active sites, increased surface area and interfacial area, superior sunlight absorption capability, and enhanced photon-capturing capability, which promoted the electrolyte diffusion and charge transfer.

These findings offer a rational design strategy for nanostructured perovskite oxides toward high-efficiency PEC water splitting.

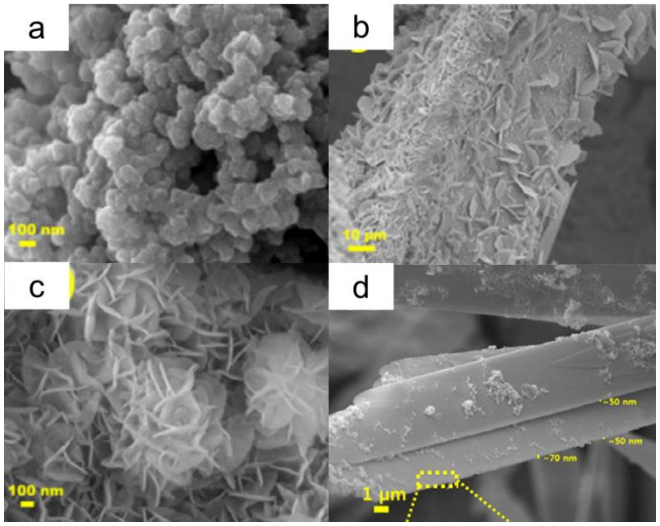

Figure 4. SEM images of PMT perovskite oxides with various morphologies. (a) Nanospheres, (b) flakes, (c) hierarchical flowers, and (d) thin microbelts. Reproduced with permission from ref. [116], Copyright 2017, Elsevier.

Hojamberdiev et al. studied the effect of A-site cation exchange on the morphology, photocatalytic HER and OER activities, and dynamics of photoinduced electron-hole pairs of $ATaON_2$ (A = La and Pr) under visible light irradiation.[117] $PrTaON_2$ crystals showed an irregular microstructure with an average particle size of 125 nm, which were strongly connected to each other, while $LaTaON_2$ crystals showed a nanorod (NR) morphology with an average length of 320 nm and a width of 100 nm. Compared to $LaTaON_2$, $PrTaON_2$ exhibited lower photocatalytic HER/OER activities and PEC performance owing to the excessive number of intrinsic defects associated with anionic vacancies, different morphologies and reduced Ta species. The above results suggest that the selection of a suitable A-site cation is important to tailor the morphology and to determine the PEC performance.

$Ba_5Ta_4O_{15}$ nanosheets-based thin films fabricated on metallic Ta substrates by an *in-situ* hydrothermal method were transformed to $BaTaO_2N$ perovskite oxynitride with branched nanostructures by thermal nitridation in NH_3 atmosphere for the application in PEC-OER.[118] Figure 5a shows a top-view SEM image of a $Ba_5Ta_4O_{15}$ nanosheets-based thin film supported on Ta substrates. The influence of the nitridation temperature on the microstructure and crystallinity of the $BaTaO_2N$ films was investigated. Figure 5b-e show top-view SEM images of $BaTaO_2N$ thin films nitrided at 850-1000 °C. The microstructure of the samples after nitridation at 850 and 900 °C was virtually identical to that of the pristine $Ba_5Ta_4O_{15}$. By contrast, following the nitridation at 950 and 1000 °C, $BaTaO_2N$ films with a branching nanostructure were formed as a result of partial breakdown of individual nanosheets. This is clearly seen in Figure 5e for a nitridation temperature of 1000 °C, where the oxide nanosheets were structurally altered to produce a $BaTaO_2N$ film, although the basic nanosheet framework was retained and no significant aggregation to form large particles occurred.[118] The sample nitrided at 1000 °C exhibited the highest photocurrent density because of a more complete phase transformation from the oxide to the oxynitride, a higher degree of crystallinity of the $BaTaO_2N$ phase and the more branched nanostructures, which reduced the particle size and facilitated the transfer of photoinduced holes to the photoelectrode surface by shortening the diffusion distance for holes. When coupled with a cobalt phosphate (CoPi) cocatalyst, the CoPi/$BaTaO_2N$ photoelectrode showed a stable photocurrent density of around 0.75 mA cm^{-2} at 1.23 V vs. RHE under simulated sunlight illumination.

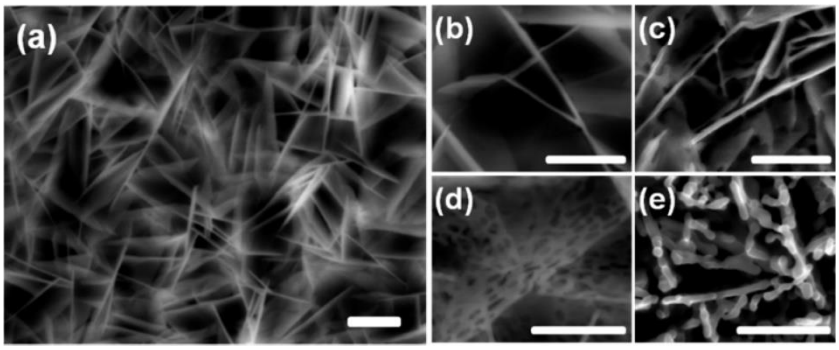

Figure 5. SEM images of (a) $Ba_5Ta_4O_{15}$ and $BaTaO_2N$ films nitrided at various temperatures (b) 850, (c) 900, (d) 950 and (e) 1000 °C. All scale bars are 500 nm. Reproduced with permission from ref. [118], Copyright 2016, American Chemical Society.

3.3. Surface Engineering

Another alternative strategy for improving the PEC activity of perovskite oxides is known as surface decoration/engineering. Surface engineering by modifications with already known and widely investigated semiconductors (*e.g.*, TiO_2, SnO_2, Fe_2O_3, WO_3 and $BiVO_4$)[35,37,38,119,120] in view of improving their activities and functionalities has been already reported. Based on the literature, there are two ways to improve the performance by using the surface engineering strategy through decoration. One is through the anchoring of a cocatalyst onto the photoelectrode to promote charge carrier separation and to facilitate hydrogen and oxygen evolution kinetics.[121,122] The other is through the surface modification by organic dyes, plasmonic materials or quantum dots (QDs), etc., to enhance the visible light absorption.[123-127] The sluggish water splitting kinetics of the perovskite oxide-based photoelectrodes can be enhanced by surface decoration of cocatalysts or other functional materials with high electrocatalytic activity and charge transfer capability.

The PEC-OER activity of $SrTiO_3$ (STO) nanocubes was enhanced by coupling with NiO nanoparticles, which was denoted as NiO@STO nanoparticle@nanocube.[128] The nanostructures and particle sizes of the pristine STO and NiO@STO composite are shown in Figure 6a-d. Cubic-like STO nanocrystals with smooth surface were observed while NiO@STO composite particles also exhibited a cubic morphology with many NiO nanoparticles on the STO surface. The phase junctions were confirmed by transmission electron microscopy (TEM) observation, as evidenced by the NiO nanoparticles intimately attached to the STO surface from the images as shown in Figure 6e, f. The photocurrent density of NiO@STO nanostructured composite reached 3.5 μA cm^{-2} at 0 V vs. Ag/AgCl, which was 7 times higher than pristine STO. The NiO@STO composite displayed a superior PEC-OER activity with an O_2 production amount of around 100 μmol after 3-hour sunlight irradiation, which was around 1.7 times higher than that of the pristine STO. The phase junctions between NiO and STO created by surface decoration accelerated the hole transportation from STO to NiO and suppressed the electron-hole recombination rate by the internal electrostatic field at the interface, which mainly contributed to the greatly improved PEC activity of the NiO@STO composite. The NiO@STO hierarchical nanostructures may have great potential in other applications such as photoelectrical devices and photocatalytic water splitting. Very recently, a new concept of site-isolation was realized by Pt solution infiltration only in the internal core of $PbTiO_3$ nanotube arrays and electrons and holes are efficiently separated on the inside and outer surface of the $PbTiO_3$ nanotubes, respectively.[129] Under visible light illumination, the site-isolated Pt-nanodot deposited $PbTiO_3$ photoanode displayed a superior PEC-OER performance to the particulate-type photoanode and the pristine $PbTiO_3$ nanotube, due primarily to the greatly enhanced electron-hole separation efficiency. This study offers a new and efficient strategy for the fabrication of PEC water splitting devices with enhanced performance.

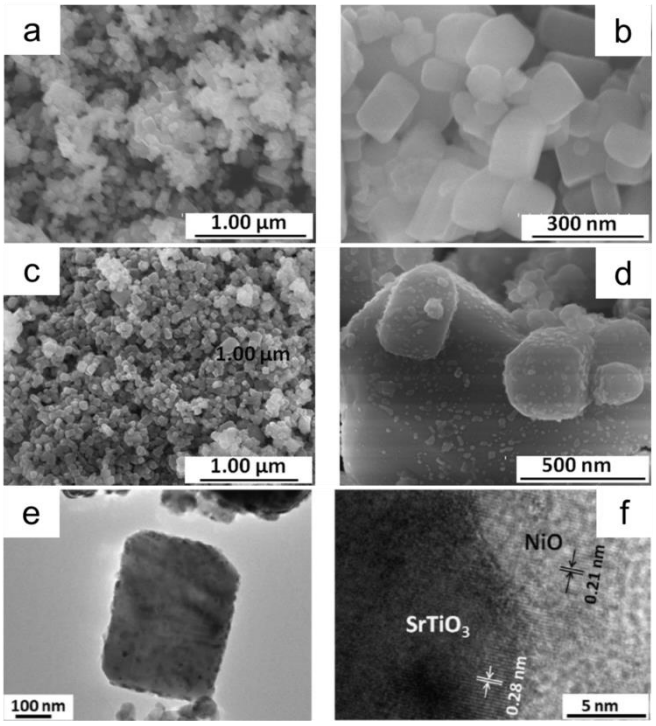

Figure 6. SEM images of (a, b) STO nanocubes and (c, d) NiO@STO nanoparticle@nanocube, TEM images of (e, f) NiO@STO hybrid. Reproduced with permission from ref. [128], Copyright 2016, Elsevier.

Besides the oxide-based surface modifiers, QDs have also been used to decorate perovskite oxides to enhance the PEC performance. For example, Wang et al. developed porous and solid STO films by a hydrothermal route using TiO_2 nanotubes as the precursor while carbon quantum dots (CQDs) were used as the functional modifiers to decorate the STO surface by an electrodeposition route.[130] Superior electron-hole transfer and separation rates were achieved by the CQD-STO composite through the interface, which contributed to its high PEC performance as shown in Figure 7. By controlling the deposition time, STO-C3 (obtained at a deposition time of 60 s) showed the highest photocurrent density of 105 μA cm^{-2}, which was much superior to that of STO and other CQD-STO composites prepared at a shorter or longer deposition time.

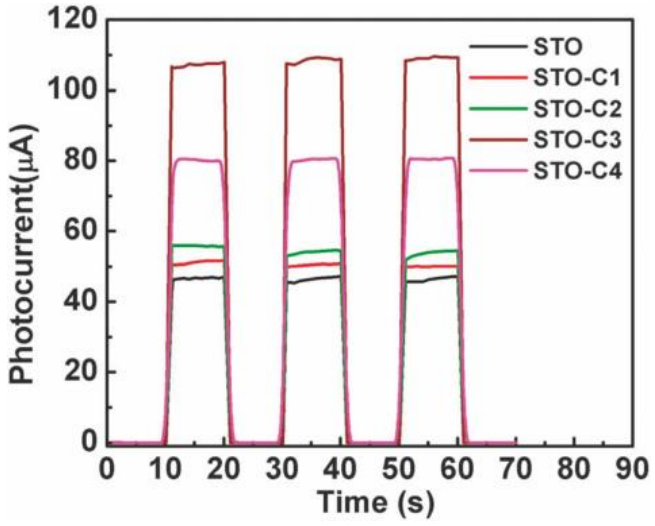

Figure 7. The *I–T* curves of pristine STO and STO films modified by CQDs with various amounts by controlling the deposition time (10 s for STO-C1, 30 s for STO-C2, 60 s for STO-C3, and 90 s for STO-C4) at 0 V vs. Ag/AgCl under simulated solar irradiation with 10 s light on/off cycles. Reproduced from Ref. [130] with permission from the Centre National de la Recherche Scientifique (CNRS) and The Royal Society of Chemistry.

More recently, CdS QD-decorated $BaSnO_3$ nanowires (NWs) were fabricated and applied as the photoanode for PEC water splitting.[131] Electrospinning and wet-chemical methods were used to prepare $BaSnO_3$ NWs and the CdS-$BaSnO_3$ composite, respectively. The amount of polyvinylpyrrolidone (PVP) played an essential role in the fabrication of $BaSnO_3$ NWs in the electrospinning process. The nanoparticles stacked $BaSnO_3$ NWs became looser with the increasing amount of PVP. The use of 11 wt.% PVP led to tightly stacked nanoparticles in the $BaSnO_3$ NWs with superior inter-crystalline connections, which promoted the electron transfer and separation processes in PEC water splitting. Figure 8 displays the nanostructure evolution of $BaSnO_3$ NWs with the optimal PVP amount of 11 wt.% and various calcination temperatures. It was found that $BaSnO_3$ NWs (850 °C) consisted of many primary nanoparticles (around 38.5 nm in diameter) and the particle size of the primary nanoparticles increased with the increase in calcination temperatures. The particle sizes were demonstrated to be 43.8, 64.3 and 430 nm at calcination temperatures of 900, 950 and 1000 °C, respectively, while some of the $BaSnO_3$ NWs were broken at high sintering temperatures. The optimized CdS QDs-decorated $BaSnO_3$ NWs hybrid photoanode exhibited a high photocurrent density of 4.8 mA cm^{-2} at 0 V (vs. saturated calomel electrode, SCE) and a H_2 production rate of 71.8 μmol h^{-1} cm^{-2}, which was attributed to the enhanced charge separation capability at the $BaSnO_3$/CdS interface. These results suggest that the CdS-$BaSnO_3$ composite is an excellent candidate for PEC water splitting and the PEC activity can be well tuned by rationally designing the interfaces and nanostructures.

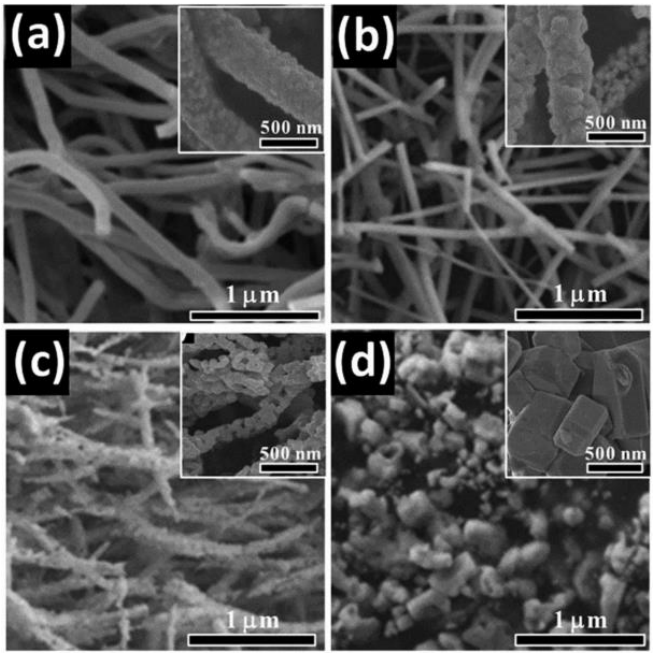

Figure 8. SEM images of $BaSnO_3$ NWs (11 wt.% PVP) with different calcination temperatures. (a) 850 °C, (b) 900 °C, (c) 950 °C, and (d) 1000 °C. Reproduced with permission from ref. [131], Copyright 2015, Royal Society of Chemistry.

3.4. Heterojunction Building

Tuning the semiconducting behaviors of the photoelectrodes is a major concern in developing PEC water splitting devices given the fact that the extent of photoexcitation and the amount of photoexcited carriers participating in the water splitting under sunlight irradiation are determined by the semiconducting behaviors of the electrodes. For a specific semiconducting material, the creation of heterojunction is important to enhance the PEC activity, promote the charge separation process as well as improve the stability under photoexcitation.[132-136] The rational construction of different metal oxides into heterostructures is very useful in promoting the separation of photo-generated carriers and in maximizing the sunlight absorption. For example, combining $BiVO_4$ and WO_3 to form a heterojunction-based composite not only promoted the separation of photo-induced charge carriers, but also enhanced the sunlight absorption capability.[39]

Nanostructured $BaTiO_3$/Cu_2O heterojunctions were built by spray deposition of porous Cu_2O films onto the nanostructured $BaTiO_3$ thin films fabricated by spin coating for the application as electrodes in PEC water splitting to produce H_2.[137] The p-n junction with various thicknesses of Cu_2O thin films provided an improved separation efficiency of the photoinduced electrons and holes and enhanced sunlight harvesting capability as compared to the single-phase electrode, which was both confirmed by experimental results and theoretical calculations. The highest photocurrent density of 1.44 mA cm^{-2} at 0.95 V vs. SCE was obtained by this composite photoelectrode with a 442

nm-thick Cu_2O layer due to optimized charge transfer capability. Through a hydrothermal process and a ferroelectric polarization-endowed band engineering strategy, a uniform, epitaxial and poled $BaTiO_3$ layer was formed on TiO_2 NWs.[138] After the optimization of the thickness of the $BaTiO_3$ coating layer, an attractive photocurrent density enhancement of 67% (1.30 vs. 0.78 mA cm^{-2}) was obtained by the 5 nm $BaTiO_3$-coated TiO_2 NWs as compared with TiO_2 NWs, which was associated with the creation of heterojunctions, the improved separation capability of the charge carriers, and the effective tuning of interfacial band structure. This research suggests that ferroelectric polarization is a useful way to tailor the PEC activity of heterojunction-based semiconducting electrodes beyond the limitation of chemical, structural and compositional optimization.

Three-dimensional (3D) heterostructures based on Sb:SnO_2 (ATO)@TiO_2-$SrTiO_3$ were created via a hydrothermal route using an ATO@TiO_2 nanobelt (NB) as the template.[139] As shown in Figure 9a and b, the ATO NBs in the ATO@TiO_2 nanostructures were covered by TiO_2 NRs composed of needle-like leaves whereas those in the ATO@TiO_2-$SrTiO_3$ sample were covered by TiO_2-$SrTiO_3$ composed of broad leaves (Figure 9c and d), suggesting that the surface TiO_2 NRs were converted to $SrTiO_3$ with a morphology change. The transformation from TiO_2 to $SrTiO_3$ was proposed to occur via a dissolution-precipitation mechanism in an alkaline solution.[140,141] TiO_2 was easily dissolved by OH^- ions with a high concentration and titanium hydroxyl species such as $HTiO_3^-$ was then formed.[142] As shown in Figure 9e, $HTiO_3^-$ was formed by the reaction between TiO_2 and OH^- ions from $Sr(OH)_2$ during the first step. After that, $SrTiO_3$ was formed by the reaction of $HTiO_3^-$ and Sr^{2+}, resulting in a hetero-nucleate on the surface of TiO_2 NRs. $SrTiO_3$ clusters accumulated with the increasing reaction time and finally a $SrTiO_3$ layer was formed on the TiO_2 NRs surface. $SrTiO_3$-encapsulated TiO_2 NRs were obtained by preventing the further growth or Oswald ripening through the control over total reaction time. It was also found that $SrTiO_3$ particles agglomerated instead of attaching with TiO_2 NRs when water was used as the solvent in the hydrothermal process, suggesting that the ethanol solvent played a key role in the particle size tuning and assembling of $SrTiO_3$ nanoparticles on TiO_2 NRs due to the different dielectric constants of ethanol and water. The ATO@TiO_2-$SrTiO_3$ hetero-structured electrode showed a superior photocurrent density compared to ATO@TiO_2 due to the blocking effect of $SrTiO_3$ layer and the shift in Fermi level. Park et al.'s work demonstrates that a synergetic effect between 3D nanoarchitecture and heterostructure is very effective in improving the PEC activity of simple and complex metal oxides.[139]

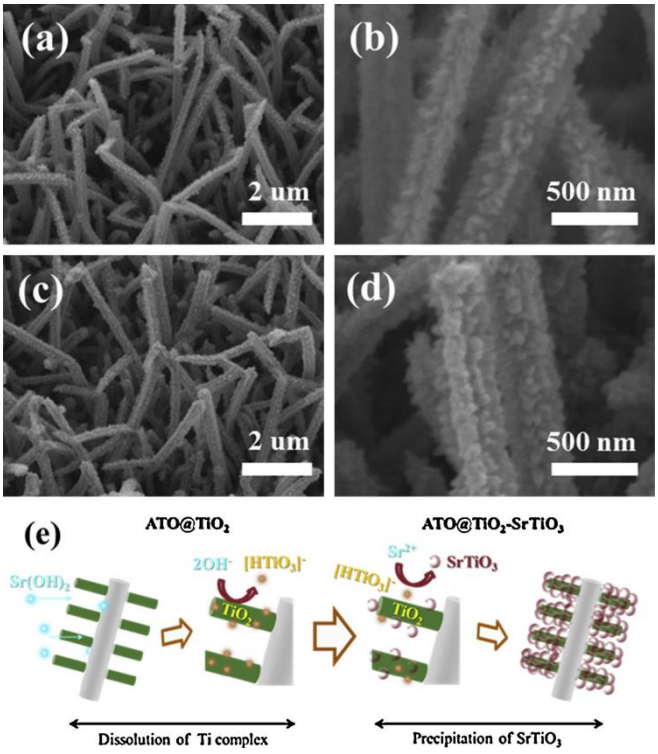

Figure 9. SEM images of (a, b) ATO@TiO_2, (c, d) ATO@TiO_2-$SrTiO_3$ arrays, and (e) a schematic formation process of ATO@TiO_2-$SrTiO_3$. Reproduced with permission from ref. [139], Copyright 2014, Elsevier.

Oxygen deficiency (vacancy) and defect control is established as a viable strategy to tailor the electronic structure and photocatalytic activity of metal oxides.[143,144] TiO_2/Bi_2WO_6 heterostructures with well-tuned electronic structures at the interface were applied to investigate the effect of interfacial oxygen vacancy on the PEC performance in water splitting.[145] This composite electrode displayed a much higher PEC performance than the pristine TiO_2 due to the suppression of intrinsic defects in Bi_2WO_6 and the rational tailoring of the sites and amounts of oxygen vacancies. As shown in Figure 10, the deposition of Bi_2WO_6 obviously improved the photoresponse as compared with the pristine TiO_2 and the photocurrent density of the TiO_2/Bi_2WO_6 heterostructures was strongly determined by the concentration of intrinsic defects in Bi_2WO_6. The R-TiO_2/L-O_v-Bi_2WO_6 composite displayed the highest PEC activity, which was around 3 times larger than that of the single-phase TiO_2. On the other hand, a slightly increased photocurrent density was obtained by the TiO_2/H-O_v-Bi_2WO_6 hybrid, implying that excessive intrinsic oxygen vacancies in Bi_2WO_6 may have a detrimental effect on the PEC activity for water splitting.[145]

Besides the intrinsic defects in Bi_2WO_6, the interfacial oxygen vacancies of TiO_2 also caused strong impact on the charge transfer and separation capability of the TiO_2/Bi_2WO_6 heterostructures. R-TiO_2/L-O_v-Bi_2WO_6 composite showed a much superior PEC activity to that of R/A-TiO_2/Bi_2WO_6 (Figure 10b), suggesting the critical role of interfacial oxygen vacancies in TiO_2.[145] The oxygen vacancies around the Bi_2WO_6/TiO_2

interface (near the TiO_2 side) had a positive effect on the migration of electrons to conducting substrates. A facile vacuum treatment process facilitated the oxygen vacancy formation and the highest PEC activity was obtained. It indicates that PEC activity of metal oxide-based photoanodes can be well tailored and enhanced by inhibiting the intrinsic defects and increasing the amount of interfacial oxygen vacancies. An et al.'s study provides some atomic-level insights into the intrinsic and interfacial defect control to enhance the PEC performance, which may present a new principle to design efficient heterostructure-based electrodes and photocatalysts for various photocatalytic applications.

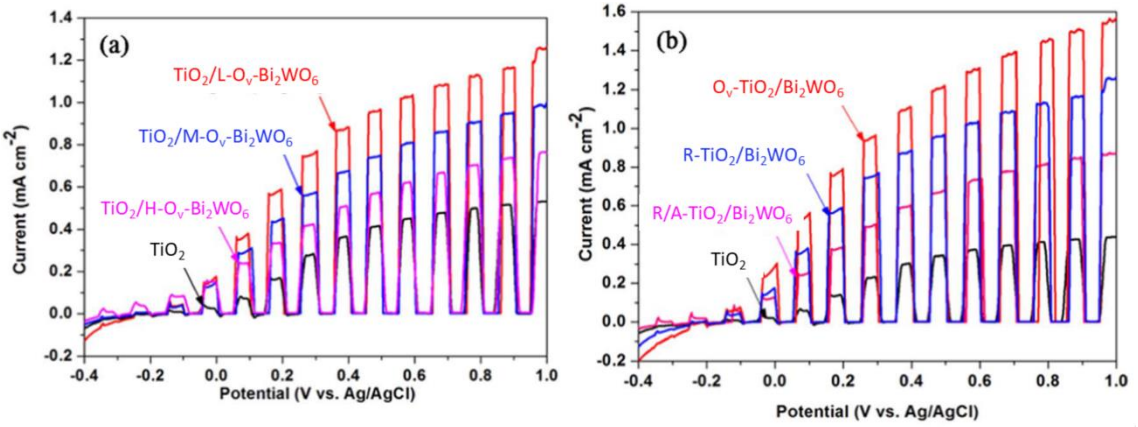

Figure 10. (a) Effect of intrinsic oxygen vacancies in Bi_2WO_6 and (b) interfacial oxygen vacancies in the hybrid on the PEC performance of photoanodes; In this figure, L-O_v-Bi_2WO_6, M-O_v-Bi_2WO_6 and H-O_v-Bi_2WO_6 are Bi_2WO_6 with low, medium and high oxygen vacancy amount, respectively. R-TiO_2, R/A-TiO_2 and O_v-TiO_2 are rutile TiO_2, rutile/anatase TiO_2 and vacuum treated rutile TiO_2, respectively. Reproduced with permission from ref. [145], Copyright 2017, Elsevier.

Besides simple metal oxides, metal sulfides have also been used to couple with perovskite oxides with the formation of heterostructures to improve the PEC activity.[146,147] Visible-light-active $NaNbO_3$/Ag_2S core-shell structured heterostructures were prepared by an ion-exchange route for PEC water splitting.[146] The $NaNbO_3$/Ag_2S heterostructures displayed a positive shift in the onset potential (1.1 V) and a high photocurrent density of 2.44 mA cm^{-2} at 0.9 V vs. Ag/AgCl, which was attributed to the efficient interfacial transfer of the charge carriers. More recently, Kumar et al. studied the influence of exposed facets and crystal structures of $NaNbO_3$ on the activity of core-shelled $NaNbO_3$/CdS heterostructures for PEC water splitting.[147] The (001) facets of the cubic phase of $NaNbO_3$ showed a much better PEC performance than that of (110) and (114) facets of the orthorhombic structured $NaNbO_3$ due to the effective spatial and inter-facet charge separation processes. Kumar et al.'s research work on facet-selective synthesis reveals the importance of the rational design of visible-light-active core-shell structured composites by stabilizing the core material with proper phase structure and microstructure to obtain much improved PEC activity.

4. Summary and Outlook

For single-phase semiconducting material-based water splitting, the band gap of the semiconductor should sandwich between the potentials of water reduction/oxidation reactions and then the photoinduced electrons and holes can possess enough and proper overpotential for the HER and OER, respectively. Several semiconductors such as TiO_2 are cost-effective and photostable but they show inferior sunlight harvesting capability due to their large band gaps, especially for the visible light. Thus, the design, development and construction of visible-light-sensitive photoelectrodes is critical. Due to the excellent structural flexibility of perovskite oxides, the application of perovskite oxides as electrodes for PEC water spitting is very essential for the achievement of high STH efficiency, although this new field is still in its infancy and faces many challenges. In this paper, we have reviewed the research advances of using perovskite oxides as photoelectrodes for PEC water splitting and the design strategies of high-performance perovskite-based PEC electrodes are presented. This review aims to give some helpful and important guidance for the future research of PEC water splitting with Earth-abundant perovskite-based electrodes.

The PEC water-splitting performance of some typical pure perovskite oxides as photoelectrodes is listed in Table 1.[96,100,102,104,106-109,115,116,118,148-153] As can be seen, the nanostructure construction, morphology control and lattice doping play critical roles in the achievement of high PEC activity while the pristine perovskites often show much lower performance. In particular, the nanostructuring methodology is very useful to enhance the PEC performance of perovskite oxide-based photoelectrodes with inferior charge carrier mobility and short excited state lifetimes by increasing the active surface area. For example, lead magnesium titanate perovskite oxides with thin microbelt morphology showed a much better PEC performance compared to lead magnesium titanate with nanospheres, flakes and hierarchical flower morphologies. On the other hand, the PEC performance is also determined by the

intrinsic parameters of perovskite materials such as chemical composition (compositional elements), conductivity, defect concentrations, etc. For most of the perovskite oxides, the low electrical conductivity/electron mobility, high defect amount and short lifetimes of charge carriers are critical issues that cannot be addressed by nanostructuring alone. Lattice doping and defect control/engineering in perovskite oxides are proved to effectively enhance the photoinduced charge carrier concentration and the electrical conductivity, while the improvement in band bending also promotes the electron-hole separation. However, poor conductivity and/or low sunlight harvesting capability are still the main limitations of most perovskite oxides for the application as the photoelectrodes in PEC water splitting alone. The co-doping with anions and cations in perovskite oxides should be a useful strategy to tailor the band gaps and electronic band structures to meet the prerequisites as electrodes in PEC water splitting. Nevertheless, the experimental progress is still unsatisfactory due to the challenges of enhancing the doping efficiency and controlling the concentration and spatial distribution of the dopants.

Surface engineering/decoration and heterojunction building/creation are two of the most investigated methods to modify perovskite oxides to improve the PEC performance by facilitating the charge separation, surface reaction kinetics and/or sunlight absorption efficiency. The PEC performance of some typical perovskite oxide-based composites/hybrids as photoelectrodes is listed in Table 2.[95,101,117,128-131,134-138,145-147,154,155] Most PEC devices with perovskite oxide-based composite photoelectrodes outperform those based on their corresponding components, which can be explained by the presence of a synergetic effect. However, the synergetic effect or interaction/coupling effect between perovskite oxides and other functional components has not been clearly understood up to now and it should be clarified in future research, and theoretical calculations may be a useful tool. QDs are thus far the most used materials to decorate the perovskite surface. For example, the use of CdS QDs improved the PEC performance of $BaSnO_3$ NWs by 10 times. Core-shell structures based on heterojunction have received more and more attention with perovskite oxides as the core or shell. For example, core-shell structured $NaNbO_3/Ag_2S$ with $NaNbO_3$ perovskite as the core showed a much improved PEC performance than that of $NaNbO_3$ or Ag_2S alone. Core-shell structured $BaTiO_3@TiO_2$ NWs with perovskite oxide $BaTiO_3$ as the shell also showed a much superior PEC activity to TiO_2 NWs. Introducing 3D conducting substrates to support perovskite oxides should be a future research direction. A 3D conducting substrate such as fluorine doped tin oxide coated glass (FTO glass), Ni foam, and carbon cloth/fiber will enhance the charge transport and collection capability, which may benefit perovskite oxides with poor charge transport capability. Furthermore, the construction of a single-crystalline structure or a polycrystalline structure with few high angle grain boundaries will be beneficial to the effective charge carrier separation/transfer in PEC water splitting process. Considering the low surface area and high intrinsic activity of perovskite oxides, forming composites with high-surface-area carbon materials may be a useful strategy to enhance the PEC performance of perovskite-based electrodes, which could provide the advantages of both perovskite oxides and carbon materials. Furthermore, a phenomenon called exsolution or precipitation of NPs has been recently observed at the surface of perovskite oxides and the NPs are particularly active for electrocatalytic OER and HER. The application of exsolution in perovskite-based electrodes for PEC water splitting should be an attractive future research direction. In addition to the design strategies of perovskite oxide-based electrodes to enhance the PEC performance, some advanced synthetic techniques can be used for the synthesis of perovskite oxide-based electrodes. For example, electrospinning technique can be easily tailored to synthesize perovskite oxide nanofibers with high surface area and superior activity. In addition, one-pot synthesis of perovskite-based heterostructures can be achievable, which may help boost the PEC performance owing to the combined benefits of multiple active components. Additionally, in most of the studies summarized in this review, the operational stability of the perovskite oxide-based photoelectrodes for PEC water splitting was seldom investigated, and the presented testing periods and performance retention are rather short. The operational stability should be a big concern for future studies.

Furthermore, some other critical issues need to be addressed to enhance the PEC performance of perovskite-based electrodes. A combined experimental and theoretical study is needed to build relationships between the structure/surface properties and the PEC activity, thus providing guidance for the rational design of novel perovskite oxide-based photoelectrodes with superior photocatalytic/electrocatalytic activity and durability. However, it is still very difficult to precisely investigate the working mechanism of complex systems (e.g., composite photoelectrode system) by using the existing methodologies although some research advances have been made in the establishment of density functional theory calculations to predict potential photoelectrodes. As a result, more efficient computational methods should be developed to well predict the possible perovskite-based photoelectrodes for highly efficient PEC water splitting.

Photoelectrodes should be very active for PEC water splitting under sunlight illumination at wavelengths of above 600 nm to meet the efficiency target of 10%.[156] Up to now, some perovskite oxide-based photocatalysts have shown considerable sunlight absorption and photocatalytic activity under sunlight irradiation at 600-740 nm.[51,157-159] In the longer future, the development of perovskite oxide-based semiconductors showing high activity under red and near-infrared sunlight regions will become more and more essential. It can be expected that many researchers will devote themselves to the design and synthesis of highly active, stable and low-cost perovskite oxide-based electrodes for PEC water splitting to obtain adequate STH efficiency although there are still some challenges in separation, purification, transportation and scale-up of solar H_2 fuel.

Table 1. Typical single-phase perovskite oxides as photoelectrodes used in PEC water splitting.

No.	Photoelectrode	Electrolyte	Photocurrent density	Stability (photocurrent retention rate)	Ref.
1	$LaFeO_3$	1 M Na_2SO_4	8.2 mA cm^{-2} at 1.7 V vs. Ag/AgCl	50% at 30 min	108
2	$SrNbO_2N$	1 M KOH	0.113 mA cm^{-2} at 1.23 V vs. RHE	/	148
3	PMTS	0.1 M Na_2SO_4	0.521 mA cm^{-2} at 1.23 V vs. RHE	/	116
4	PMTF		0.513 mA cm^{-2} at 1.23 V vs. RHE	/	
5	PMTH		1.18 mA cm^{-2} at 1.23 V vs. RHE	/	
6	PMTT		1.77 mA cm^{-2} at 1.23 V vs. RHE	/	
7	$LaFeO_3$	0.1 M NaOH	0.1 mA cm^{-2} at 0.73 V vs. RHE	Stable for 60 min	107
8	$LaFeO_3$	0.1 M NaOH	-0.01 mA cm^{-2} at -0.25 V vs. Ag/AgCl	/	106
9	$LaFe_{0.95}Mg_{0.05}O_3$		-0.06 mA cm^{-2} at -0.25 V vs. Ag/AgCl	/	
10	$LaFe_{0.95}Zn_{0.05}O_3$		-0.05 mA cm^{-2} at -0.25 V vs. Ag/AgCl	/	
11	$CeFeO_3$	1 M NaOH	6.9 mA cm^{-2} at 1.5 V vs. Ag/AgCl	/	149
12	$BiFeO_3$	1 M NaOH	0.09 mA cm^{-2} at 1.6 V vs. RHE	/	96
13	Ti doped $BiFeO_3$		0.13 mA cm^{-2} at 1.6 V vs. RHE	/	
14	Mo doped $BiFeO_3$		0.08 mA cm^{-2} at 1.6 V vs. RHE	/	
15	Co doped $BiFeO_3$		0.05 mA cm^{-2} at 1.6 V vs. RHE	/	
16	Sn doped $BiFeO_3$		0.06 mA cm^{-2} at 1.6 V vs. RHE	/	
17	Mesoporous $SrTiO_3$	0.5 M NaOH	0.3 mA cm^{-2} at 1.0 V vs. Ag/AgCl	/	115
18	$SrTaO_2N$	1 M NaOH	0.3 mA cm^{-2} at 1.23 V vs. RHE	/	102
19	H_2 treated $SrTaO_2N$		1.1 mA cm^{-2} at 1.23 V vs. RHE	50% after 60 min	
20	$SrNbO_2N$	0.2 M Na_2SO_4 + NaOH	1.5 mA cm^{-2} at 1.23 V vs. RHE	/	150
21	$BiFeO_3$	0.2 M Na_2SO_4	0.23 μA cm^{-2} at 0.8 V vs. Ag/AgCl	/	151
22	H_2 treated $BiFeO_3$		0.69 μA cm^{-2} at 0.8 V vs. Ag/AgCl		
23	$BaTaO_2N$ nanosheets	0.5 M K_3PO_4	0.2 mA cm^{-2} at 1.23 V vs. RHE	Stable for 65 min	118
24	$BaNbO_2N$	0.5 M H_3BO_3 + KOH	0.85 mA cm^{-2} at 1.23 V vs. RHE	/	104
25	$LaFeO_3$	0.1 M KOH	0.30 mA cm^{-2} at 1 V vs. Ag/AgCl	/	109
26	$LaFe_{0.9}Cu_{0.1}O_3$		0.99 mA cm^{-2} at 1 V vs. Ag/AgCl	/	
27	$LaFe_{0.9}Co_{0.1}O_3$		0.85 mA cm^{-2} at 1 V vs. Ag/AgCl	/	
28	$LaFe_{0.9}Mn_{0.1}O_3$		0.52 mA cm^{-2} at 1 V vs. Ag/AgCl	/	
29	$BiFeO_3$	0.2 M Na_2SO_4	0.18 mA cm^{-2} at 1 V vs. Ag/AgCl	Stable for 3 h	152
30	$LaTiO_2N$	1 M Na_2SO_4 + NaOH	3.0 mA cm^{-2} at 1.23 V vs. RHE	0% after 30 min	153
31	$BaTaO_2N$	0.1 M Na_2HPO_4 + 0.1 M NaH_2PO_4	0.12 mA cm^{-2} at 1.2 V vs. RHE	/	100
32	H_2 treated $BaTaO_2N$		0.46 mA cm^{-2} at 1.2 V vs. RHE	Stable for 1 h	

Table 2. Typical perovskite oxide-based composites as photoelectrodes used in PEC water splitting.

No.	Photoelectrode	Electrolyte	Photocurrent density	Stability (photocurrent retention rate)	Ref.
1	$PbTiO_3$	1 M KOH	8 μA cm^{-2} at 1.05 V vs. RHE	/	129
2	Pt nanodots-$PbTiO_3$		64 μA cm^{-2} at 1.05 V vs. RHE	/	
3	CoPi-$LaTaON_2$	1 M KOH	0.33 mA cm^{-2} at 1.23 V vs. RHE	/	117
4	CoPi-$PrTaON_2$		0.21 mA cm^{-2} at 1.23 V vs. RHE	/	
5	TiO_2	0.2 M Na_2SO_4	0.4 mA cm^{-2} at 1 V vs. Ag/AgCl	/	145

6	TiO_2/Bi_2WO_6	1 M NaOH	1.58 mA cm^{-2} at 1 V vs. Ag/AgCl	/	136
7	Fe_2O_3 NRs		0.37 mA cm^{-2} at 1.23 V vs. RHE	/	
8	Fe_2O_3 NRs + $LaFeO_3$		0.58 mA cm^{-2} at 1.23 V vs. RHE	/	
9	o-$NaNbO_3$	0.5 M Na_2SO_4	~0 mA cm^{-2} at 1 V vs. Ag/AgCl	/	147
10	c-$NaNbO_3$		0.13 mA cm^{-2} at 1 V vs. Ag/AgCl	/	
11	o-$NaNbO_3$/CdS		0.40 mA cm^{-2} at 1 V vs. Ag/AgCl	/	
12	c-$NaNbO_3$/CdS		2.05 mA cm^{-2} at 1 V vs. Ag/AgCl	Stable for 3 h	
13	TiO_2	0.1 M KOH	0.04 mA cm^{-2} at 1.23 V vs. RHE	/	135
14	$PbTiO_3$		0.01 mA cm^{-2} at 1.23 V vs. RHE	/	
15	Core shell TiO_2@$PbTiO_3$		0.30 mA cm^{-2} at 1.23 V vs. RHE	/	
16	$SrTiO_3$ nanotube (NT)	0.1 M Na_2SO_4	0.5 μA cm^{-2} at 0 V vs. RHE	/	128
17	NiO@$SrTiO_3$ NT		3.5 μA cm^{-2} at 0 V vs. RHE	/	
18	CoPi-La(Ta, Nb)O_2N	0.2 M K_3PO_4 + KOH	20.0 mA cm^{-2} at 1.23 V vs. RHE	50% after 35 min	95
19	Ag_2S	0.5 M Na_2SO_4	0.60 mA cm^{-2} at 0.9 V vs. Ag/AgCl	/	146
20	$NaNbO_3$		0.038 mA cm^{-2} at 0.9 V vs. Ag/AgCl	/	
21	Core shell $NaNbO_3/Ag_2S$		2.44 mA cm^{-2} at 0.9 V vs. Ag/AgCl	/	
22	$BaTiO_3$	0.1 NaOH	0.02 mA cm^{-2} at 0.95 V vs. SCE	/	137
23	$BaTiO_3/Cu_2O$		1.44 mA cm^{-2} at 0.95 V vs. SCE	/	
24	TiO_2 NWs	1 M NaOH	0.78 mA cm^{-2} at 1.23 V vs. RHE	/	138
25	$BaTiO_3$ coated TiO_2 NWs		1.30 mA cm^{-2} at 1.23 V vs. RHE	/	
26	$BaSnO_3$ NWs	0.25 M Na_2S + 0.35 M Na_2SO_3	0.5 mA cm^{-2} at 0 V vs. SCE	/	131
27	CdS QDs-$BaSnO_3$ NWs		4.8 mA cm^{-2} at 0 V vs. SCE	/	
28	STO-$BiFeO_3$ (1:9)	0.5 M phosphate solution	0.2 mA cm^{-2} at 0 V vs. RHE	/	154
29	STO-$BiFeO_3$ (1:3)		0.33 mA cm^{-2} at 1.23 V vs. RHE	Stable for 3 h	
30	STO-$BiFeO_3$ (1:1)		~0.2 mA cm^{-2} at 1.23 V vs. RHE	/	
31	STO-$BiFeO_3$ (3:1)		~0.07 mA cm^{-2} at 1.23 V vs. RHE	/	
32	Co metal/$BaTaO_2N$	0.2 M K_3PO_4	4.2 mA cm^{-2} at 1.2 V vs. RHE	80% after 6 h	101
33	$Co_3O_4/LaTiO_2N$	1 M NaOH	4.0 mA cm^{-2} at 1.23 V vs. RHE	33% after 2.5 h	155
34	Cu_2O	0.1 M NaOH	0.1 mA cm^{-2} at 0.8 V vs. SCE	/	134
35	$Cu_2O/SrTiO_3$		2.52 mA cm^{-2} at 0.8 V vs. SCE	/	
36	$SrTiO_3$	0.1 M Na_2SO_4	0.045 mA cm^{-2} at 0 V vs. Ag/AgCl	/	130
37	CQDs-$SrTiO_3$		0.105 mA cm^{-2} at 0 V vs. Ag/AgCl	/	

Acknowledgements

This work is supported by Australian Research Council Discovery Projects under contracts DP150104365 and DP160104835, Program for Jiangsu Specially-Appointed Professors and the Funding from State Key Laboratory of Materials-Oriented Chemical Engineering (No. ZK201808).

Keywords: photoelectrochemical water splitting • perovskite oxide • photoelectrodes • hydrogen evolution reaction • oxygen evolution reaction

[1] S. E. Hosseini, M. A. Wahid, *Renew. Sust. Energ. Rev.* **2016**, *57*, 850-866.

[2] A. Vita, C. Italiano, L. Pino, M. Laganà, V. Recupero, *Appl. Catal. B: Environ.* **2017**, *218*, 317-326.

[3] W. Wang, H. Zhu, G. Yang, H. J. Park, D. W. Jung, C. Kwak, Z. Shao, *J. Power Sources* **2014**, *258*, 134-141.

[4] K. Jordal, R. Anantharaman, T. A. Peters, D. Berstad, J. Morud, P. Nekså, R. Bredesen, *Energy* **2015**, *88*, 9-17.

[5] G. Chen, Z. Hu, Y. Zhu, B. Gu, Y. Zhong, H.-J. Lin, C.-T. Chen, W. Zhou, Z. Shao, *Adv. Mater.* **2018**, *30*, 1804333.

[6] X. Li, S. Liu, K. Fan, Z. Liu, B. Song, J. Yu, *Adv. Energy Mater.* **2018**, *8*, 1800101.

[7] K. Oka, O. Tsujimura, T. Suga, H. Nishide, B. Winther-Jensen, *Energy Environ. Sci.* **2018**, *11*, 1335-1342.

[8] C. Zhu, A.-L. Wang, W. Xiao, D. Chao, X. Zhang, N. H. Tiep, S. Chen, J. Kang, X. Wang, J. Ding, J. Wang, H. Zhang, H. J. Fan, *Adv. Mater.* **2018**, *30*, 1705516.

[9] W. Wang, X. Xu, W. Zhou, Z. Shao, *Adv. Sci.* **2017**, *4*, 1600371.

[10] J. Barber, *Chem. Soc. Rev.* **2009**, *38*, 185-196.

[11] C. Acar, I. Dincer, G. F. Naterer, *Int. J. Energy Res.* **2016**, *40*, 1449-1473.
[12] P. Li, X. Chen, H. He, X. Zhou, Y. Zhou, Z. Zou, *Adv. Mater.* **2018**, *30*, 1703119.
[13] C. N. R. Rao, S. Dey, *PNAS* **2017**, *114*, 13385-13393.
[14] H. I. Villafán-Vidales, C. A. Arancibia-Bulnes, D. Riveros-Rosas, H. Romero-Paredes, C. A. Estrada, *Renew. Sust. Energ. Rev.* **2017**, *75*, 894-908.
[15] D. Marxer, P. Furler, M. Takacs, A. Steinfeld, *Energy Environ. Sci.* **2017**, *10*, 1142-1149.
[16] Y. Guo, T. Wang, J. Chen, J. Zheng, X. Li, K. K. Ostrikov, *Adv. Energy Mater.* **2018**, *8*, 1800085.
[17] R. Lin, H. Lei, D. Ruan, K. Jiang, X. Yu, Z. Wang, W. Mai, H. Yan, *Nano Energy* **2019**, *56*, 82-91.
[18] Y. Hou, M. Qiu, T. Zhang, J. Ma, S. Liu, X. Zhuang, C. Yuan, X. Feng, *Adv. Mater.* **2017**, *29*, 1604480.
[19] C.-Y. Lee, A. C. Taylor, S. Beirne, G. G. Wallace, *Adv. Energy Mater.* **2017**, *7*, 1701060.
[20] I. Roger, M. A. Shipman, M. D. Symes, *Nat. Rev. Chem.* **2017**, *1*, 0003.
[21] X. Xu, W. Wang, W. Zhou, Z. Shao, *Small Methods* **2018**, *2*, 1800071.
[22] D. Li, J. Shi, C. Li, *Small* **2018**, *14*, 1704179.
[23] W. Wang, M. O. Tade, Z. Shao, *Chem. Soc. Rev.* **2015**, *44*, 5371-5408.
[24] S. Wang, T. He, J.-H. Yun, Y. Hu, M. Xiao, A. Du, L. Wang, *Adv. Funct. Mater.* **2018***, 28,* 1802685*.*
[25] A. Landman, H. Dotan, G. E. Shter, M. Wullenkord, A. Houaijia, A. Maljusch, G. S. Grader, A. Rothschild, *Nat. Mater.* **2017**, *16*, 646-652.
[26] Z. Zhang, C. Gao, Y. Li, W. Han, W. Fu, Y. He, E. Xie, *Nano Energy* **2016**, *30*, 892-899.
[27] K.-H. Ye, Z. Wang, J. Gu, S. Xiao, Y. Yuan, Y. Zhu, Y. Zhang, W. Mai, S. Yang, *Energy Environ. Sci.* **2017**, *10*, 772-779.
[28] T. Butburee, Y. Bai, H. Wang, H. Chen, Z. Wang, G. Liu, J. Zou, P. Khemthong, G. Q. M. Lu, L. Wang, *Adv. Mater.* **2018**, *30*, 1705666.
[29] J. Zhang, H. Ma, Z. Liu, *Appl. Catal. B: Environ.* **2017**, *201*, 84-91.
[30] J. S. Kang, Y. Noh, J. Kim, H. Choi, T. H. Jeon, D. Ahn, J.-Y. Kim, S.-H. Yu, H. Park, J.-H. Yum, W. Choi, D. C. Dunand, H. Choe, Y.-E. Sung, *Angew. Chem. Int. Ed.* **2017**, *56*, 6583-6588.
[31] Y. Hou, M. Qiu, G. Nam, M. G. Kim, T. Zhang, K. Liu, X. Zhuang, J. Cho, C. Yuan, X. Feng, *Nano Lett.* **2017**, *17*, 4202-4209.
[32] Y. Fu, F. Cao, F. Wu, Z. Diao, J. Chen, S. Shen, L. Li, *Adv. Funct. Mater.* **2018**, *28*, 1706785.
[33] M. Zhong, T. Hisatomi, Y. Sasaki, S. Suzuki, K. Teshima, M. Nakabayashi, N. Shibata, H. Nishiyama, M. Katayama, T. Yamada, K. Domen, *Angew. Chem. Int. Ed.* **2017**, *56*, 4739-4743.
[34] P. Varadhan, H.-C. Fu, D. Priante, J. R. D. Retamal, C. Zhao, M. Ebaid, T. K. Ng, I. Ajia, S. Mitra, I. S. Roqan, B. S. Ooi, J.-H. He, *Nano Lett.* **2017**, *17*, 1520-1528.
[35] W. Chen, T. Wang, J. Xue, S. Li, Z. Wang, S. Sun, *Small* **2017**, 1602420.
[36] X. Li, S. Liu, K. Fan, Z. Liu, B. Song, J. Yu, *Adv. Energy Mater.* **2018**, *8*, 1800101.
[37] Z. Zhang, C. Gao, Z. Wu, W. Han, Y. Wang, W. Fu, X. Li, E. Xie, *Nano Energy* **2016**, *19*, 318-327.
[38] Y.-F. Xu, H.-S. Rao, B.-X. Chen, Y. Lin, H.-Y. Chen, D.-B. Kuang, C.-Y. Su, *Adv. Sci.* **2015**, *2*, 1500049.
[39] Y. Zhou, L. Zhang, L. Lin, B. R. Wygant, Y. Liu, Y. Zhu, Y. Zheng, C. B. Mullins, Y. Zhao, X. Zhang, G. Yu, *Nano Lett.* **2017**, *17*, 8012-8017.
[40] S. Wang, P. Chen, Y. Bai, J.-H. Yun, G. Liu, L. Wang, *Adv. Mater.* **2018**, *30*, 1800486.
[41] P. Tan, M. Liu, Z. Shao, M. Ni, *Adv. Energy Mater.* **2017**, *7*, 1602674.
[42] W. Wang, M. O. Tadé, Z. Shao, *Prog. Mater. Sci.* **2018**, *92*, 33-63.
[43] A. B. Murphy, P. R. F. Barnes, L. K. Randeniya, I. C. Plumb, I. E. Grey, M. D. Horne, J. A. Glasscock, *Int. J. Hydrogen Energy* **2006**, *31*, 1999-2017.
[44] Z. Chen, T. F. Jaramillo, T. G. Deutsch, A. Kleiman-Shwarsctein, A. J. Forman, N. Gaillard, R. Garland, K. Takanabe, C. Heske, M. Sunkara, E. W. McFarland, K. Domen, E. L. Miller, J. A. Turner, H. N. Dinh, *J. Mater. Res.* **2010**, *25*, 3-16.
[45] M. S. Prévot, K. Sivula, *J. Phys. Chem. C* **2013**, *117*, 17879-17893.
[46] H. Fujito, H. Kunioku, D. Kato, H. Suzuki, M. Higashi, H. Kageyama, R. Abe, *J. Am. Chem. Soc.* **2016**, *138*, 2082-2085.
[47] H. Suzuki, O. Tomita, M. Higashi, A. Nakada, R. Abe, *Appl. Catal. B: Environ.* **2018**, *232*, 49-54.
[48] F.-F. Li, D.-R. Liu, G.-M. Gao, B. Xue, Y.-S. Jiang, *Appl. Catal. B: Environ.* **2015**, *166-167*, 104-111.
[49] H. Kunioku, M. Higashi, O. Tomita, M. Yabuuchi, D. Kato, H. Fujito, H. Kageyama, R. Abe, *J. Mater. Chem. A* **2018**, *6*, 3100-3107.
[50] G. Zhang, G. Liu, L. Wang, J. T. S. Irvine, *Chem. Soc. Rev.* **2016**, *45*, 5951-5984.
[51] X. Sun, Y. Mi, F. Jiao, X. Xu, *ACS Catal.* **2018**, *8*, 3209-3221.
[52] T. Alammar, I. I. Slowing, J. Anderegg, A.-V. Mudring, *ChemSusChem* **2017**, *10*, 3387-3401.
[53] Y. Zhu, W. Zhou, J. Yu, Y. Chen, M. Liu, Z. Shao, *Chem. Mater.* **2016**, *28*, 1691-1697.
[54] C.-F. Chen, G. King, R. M. Dickerson, P. A. Papin, S. Gupta, W. R. Kellogg, G. Wu, *Nano Energy* **2015**, *13*, 423-432.
[55] T. Hisatomi, J. Kubota, K. Domen, *Chem. Soc. Rev.* **2014**, *43*, 7520-7535.
[56] F. E. Osterloh, *Chem. Soc. Rev.* **2013**, *42*, 2294-2320.
[57] Y. Hou, X. Zhuang, X. Feng, *Small Methods* **2017**, *1*, 1700090.
[58] H. Chen, S. Yang, *Nanoscale Horiz.* **2016**, *1*, 96-108.
[59] Y. Yang, S. Niu, D. Han, T. Liu, G. Wang, Y. Li, *Adv. Energy Mater.* **2017**, *7*, 1700555.
[60] Y. W. Phuan, W.-J. Ong, M. N. Chong, J. D. Ocon, *J. Photochem. Photobiol.: Photochem. Rev.* **2017**, *33*, 54-82.
[61] A. G. Tamirat, J. Rick, A. A. Dubale, W.-N. Su, B.-J. Hwang, *Nanoscale Horiz.* **2016**, *1*, 243-267.
[62] Y. Wang, H. Suzuki, J. Xie, O. Tomita, D. J. Martin, M. Higashi, D. Kong, R. Abe, J. Tang, *Chem. Rev.* **2018**, *118*, 5201-5241.
[63] M. G. Walter, E. L. Warren, J. R. McKone, S. W. Boettcher, Q. Mi, E. A. Santori, N. S. Lewis, *Chem. Rev.* **2010,** *110,* 6446-6473.
[64] J.-P. Zou, L.-Z. Zhang, S.-L. Luo, L.-H. Leng, X.-B. Luo, M.-J. Zhang, Y. Luo, G.-C. Guo, *Int. J. Hydrogen Energy* **2012**, *37*, 17068-17077.
[65] D. W. Hwang, H. G. Kim, J. S. Lee, J. Kim, W. Li, S. H. Oh, *J. Phys. Chem. B* **2005**, *109*, 2093-2102.
[66] A. Mukherji, C. Sun, S. C Smith, G. Q. Lu, L. Wang, *J. Phys. Chem. C* **2011**, *115*, 15674-15678.
[67] S. Choi, S. Park, J. Shin, G. Kim, *J. Mater. Chem. A* **2015**, *3*, 6088-6095.
[68] S. P. Jiang, L. Liu, K. P. Ong, P. Wu, J. Li, J. Pu, *J. Power Sources* **2008**, *176*, 82-89.
[69] M. Li, W. Zhou, X. Xu, Z. Zhu, *J. Mater. Chem. A* **2013**, *1*, 13632-13639.
[70] J. M. Porras-Vazquez, T. F. Kemp, J. V. Hanna, P. R. Slater, *J. Mater. Chem.* **2012**, *22*, 8287-8293.
[71] Y. Zhu, W. Zhou, J. Sunarso, Y. Zhong, Z. Shao, *Adv. Funct. Mater.* **2016**, *26*, 5862-5872.
[72] D.-G. Lee, O. Gwon, H.-S. Park, S. H. Kim, J. Yang, S. K. Kwak, G. Kim, H.-K. Song, *Angew. Chem. Int. Ed.* **2015**, *54*, 15730-15733.
[73] D. Chen, Z. Liu, Z. Guo, W. Yan, Y. Xin, *J. Mater. Chem. A* **2018**, *6*, 20393-20401.
[74] X. Han, X. Wu, Y. Deng, J. Liu, J. Lu, C. Zhong, W. Hu, *Adv. Energy Mater.* **2018**, *8*, 1800935.
[75] W. Sun, Z. Wang, W. Q. Zaman, Z. Zhou, L. Cao, X.-Q. Gong, J. Yang, *Chem. Commun.* **2018**, *54*, 996-999.
[76] J. Liu, Y. Zheng, Y. Jiao, Z. Wang, Z. Lu, A. Vasileff, S.-Z. Qiao, *Small* **2018**, *14*, 1704073.
[77] X. Xu, Y. Chen, W. Zhou, Z. Zhu, C. Su, M. Liu, Z. Shao, *Adv. Mater.* **2016**, *28*, 6442-6448.
[78] B. Hua, M. Li, W. Pang, W. Tang, S. Zhao, Z. Jin, Y. Zeng, B. S. Amirkhiz, J.-L. Luo, *Chem* **2018**, *4*, 2902-2916.

[79] X. Li, J. Zhang, Q. Feng, C. Pu, L. Zhang, M. Hu, X. Zhou, X. Zhong, W. Yi, J. Tang, Z. Li, X. Zhao, H. Li, B. Xu, *J. Mater. Chem. A* **2018**, *6*, 17288-17296.

[80] Y. Tong, J. Wu, P. Chen, H. Liu, W. Chu, C. Wu, Y. Xie, *J. Am. Chem. Soc.* **2018**, *140*, 11165-11169.

[81] J. Wang, Y. Gao, D. Chen, J. Liu, Z. Zhang, Z. Shao, F. Ciucci, *ACS Catal.* **2018**, *8*, 364-371.

[82] Y. Chen, H. Li, J. Wang, Y. Du, S. Xi, Y. Sun, M. Sherburne, J. W. Ager III, A. C. Fisher, Z. J. Xu, *Nat. Commun.* **2019**, *10*, 572.

[83] A. Galal, N. F. Atta, S. M. Ali, *Electrochim. Acta* **2011**, *56*, 5722-5730.

[84] A. Galal, H. K. Hassan, N. F. Atta, T. Jacob, *ChemistrySelect* **2017**, *2*, 10261-10270.

[85] B. E. Hayden, F. K. Rogers, *J. Electroanal. Chem.* **2018**, *819*, 275-282.

[86] Z. Li, L. Lv, J. Wang, X. Ao, Y. Ruan, D. Zha, G. Hong, Q. Wu, Y. Lan, C. Wang, J. Jiang, M. Liu, *Nano Energy* **2018**, *47*, 199-209.

[87] S. She, J. Yu, W. Tang, Y. Zhu, Y. Chen, J. Sunarso, W. Zhou, Z. Shao, *ACS Appl. Mater. Interfaces* **2018**, *10*, 11715-11721.

[88] N. F. Atta, A. Galal, S. M. Ali, *Int. J. Electrochem. Sci.* **2014**, *9*, 2132-2148.

[89] K. A. Stoerzinger, L. Wang, Y. Ye, M. E. Bowden, E. Crumlin, Y. Du, S. A. Chambers, *J. Mater. Chem. A* **2018**, *6*, 22170-22178.

[90] G. Wang, H. Wang, Y. Ling, Y. Tang, X. Yang, R. C. Fitzmorris, C. Wang, J. Z. Zhang, Y. Li, *Nano Lett.* **2011**, *11*, 3026-3033.

[91] K. Iwashina, A. Kudo, *J. Am. Chem. Soc.* **2011**, *133*, 13272-13275.

[92] S. Kawasaki, K. Nakatsuji, J. Yoshinobu, F. Komori, R. Takahashi, M. Lippmaa, K. Mase, A. Kudo, *Appl. Phys. Lett.* **2012**, *101*, 033910.

[93] L. Zhao, L. Fang, W. Dong, F. Zheng, M. Shen, T. Wu, *Appl. Phys. Lett.* **2013**, *102*, 121905.

[94] K. Cherifi, N. Allalou, G. Rekhila, M. Trari, Y. Bessekhouad, *Mater. Sci. Semicond. Process.* **2015**, *30*, 571-577.

[95] P. Arunachalam, A. Al-Mayouf, M. A. Ghanem, M. N. Shaddad, M. T. Weller, *Int. J. Hydrogen Energy* **2016**, *41*, 11644-11652.

[96] N. Rong, M. Chu, Y. Tang, C. Zhang, X. Cui, H. He, Y. Zhang, P. Xiao, *J. Mater. Sci.* **2016**, *51*, 5712-5723.

[97] S. Upadhyay, J. Shrivastava, A. Solanki, S. Choudhary, V. Sharma, P Kumar, N. Singh, V. R. Satsangi, R. Shrivastav, U. V. Waghmare, S. Dass, *J. Phys. Chem. C* **2011**, *115*, 24373-24380.

[98] K. Maeda, M. Higashi, B. Siritanaratkul, R. Abe, K. Domen, *J. Am. Chem. Soc.* **2011**, *133*, 12334-12337.

[99] A. E. Maegli, T. Hisatomi, E. H. Otal, S. Yoon, S. Pokrant, M.l Grätzel, A. Weidenkaff, *J. Mater. Chem.* **2012**, *22*, 17906-17913.

[100] M. Higashi, K. Domen, R. Abe, *J. Am. Chem. Soc.* **2013**, *135*, 10238-10241.

[101] K. Ueda, T. Minegishi, J. Clune, M. Nakabayashi, T. Hisatomi, H Nishiyama, M. Katayama, N. Shibata, J. Kubota, T. Yamada, K. Domen, *J. Am. Chem. Soc.* **2015**, *137*, 2227-2230.

[102] Y. Zhong, Z. Li, X. Zhao, T. Fang, H. Huang, Q. Qian, X. Chang, P. Wang, S. Yan, Z. Yu, Z. Zou, *Adv. Funct. Mater.* **2016**, *26*, 7156-7163.

[103] F. Wu, G. Liu, X. Xu, *J. Catal.* **2017**, *346*, 10-20.

[104] J. Seo, Y. Moriya, M. Kodera, T. Hisatomi, T. Minegishi, M. Katayama, K. Domen, *Chem. Mater.* **2016**, *28*, 6869-6876.

[105] B. Siritanaratkul, K. Maeda, T. Hisatomi, K. Domen, *ChemSusChem* **2011**, *4*, 74-78.

[106] M. I. Díez-García, R. Gómez, *ChemSusChem* **2017**, *10*, 2457-2463.

[107] G. P. Wheeler, K.-S. Choi, *ACS Energy Lett.* **2017**, *2*, 2378-2382.

[108] I. M. Nassar, S. Wu, L. Li, X. Li, *ChemistrySelect* **2018**, *3*, 968-972.

[109] Q. Peng, B. Shan, Y. Wen, R. Chen, *Int. J. Hydrogen Energy* **2015**, *40*, 15423-15431.

[110] X. Feng, Y. Chen, Z. Qin, M. Wang, L. Guo, *ACS Appl. Mater. Interfaces* **2016**, *8*, 18089-18096.

[111] C. Zhang, M. Shao, F. Ning, S. Xu, Z. Li, M. Wei, D. G. Evans, X. Duan, *Nano Energy* **2015**, *12*, 231-239.

[112] H. Han, S. Kment, F. Karlicky, L. Wang, A. Naldoni, P. Schmuki, R. Zboril, *Small* **2018**, *14*, 1703860.

[113] J. Luo, L. Steier, M.-K. Son, M. Schreier, M. T. Mayer, M. Grätzel, *Nano Lett.* **2016**, *16*, 1848-1857.

[114] S. S. M. Bhat, H. W. Jang, *ChemSusChem* **2017**, *10*, 3001-3018.

[115] A. L. Sangle, S. Singh, J. Jian, S. R. Bajpe, H. Wang, N. Khare, J. L. MacManus-Driscoll, *Nano Lett.* **2016**, *16*, 7338-7345.

[116] S. Chandrasekaran, E. J. Kim, J. S. Chung, I.-K. Yoo, V. Senthilkumar,Y. S. Kim, C. R. Bowen, V. Adamaki, S. H. Hur, *Chem. Eng. J.* **2017**, *309*, 682-690.

[117] M. Hojamberdiev, M. F. Bekheet, J. N. Hart, J. J. M. Vequizo, A. Yamakata, K. Yubuta, A. Gurlo, M. Hasegawa, K. Domen, K. Teshima, *Phys. Chem. Chem. Phys.* **2017**, *19*, 22210-22220.

[118] C. Wang, T. Hisatomi, T. Minegishi, Q. Wang, M. Zhong, M. Katayama, J. Kubota, K. Domen, *J. Phys. Chem. C* **2016**, *120*, 15758-15764.

[119] X. Fan, B. Gao, T. Wang, X. Huang, H. Gong, H. Xue, H. Guo, L. Song, W. Xia, J. He, *Appl. Catal. A: Gen.* **2016**, *528*, 52-58.

[120] M. Zhong, T. Hisatomi, Y. Kuang, J. Zhao, M. Liu, A. Iwase, Q. Jia, H. Nishiyama, T. Minegishi, M. Nakabayashi, N. Shibata, R. Niishiro, C. Katayama, H. Shibano, M. Katayama, A. Kudo, T. Yamada, K. Domen, *J. Am. Chem. Soc.* **2015**, *137*, 5053-5060.

[121] L. Wang, F. Dionigi, N. T. Nguyen, R. Kirchgeorg, M. Gliech, S. Grigorescu, P. Strasser, P. Schmuki, *Chem. Mater.* **2015**, *27*, 2360-2366.

[122] Z. Wang, G. Liu, C. Ding, Z. Chen, F. Zhang, J. Shi, C. Li, *J. Phys. Chem. C* **2015**, *119*, 19607-19612.

[123] F. Li, K. Fan, B. Xu, E. Gabrielsson, Q. Daniel, L. Li, L. Sun, *J. Am. Chem. Soc.* **2015**, *137*, 9153-9159.

[124] X. Zhang, Y. Liu, Z. Kang, *ACS Appl. Mater. Interfaces* **2014**, *6*, 4480-4489.

[125] J. Li, X. Gao, B. Liu, Q. Feng, X.-B. Li, M.-Y. Huang, Z. Liu, J. Zhang, C.-H. Tung, L.-Z. Wu, *J. Am. Chem. Soc.* **2016**, *138*, 3954-3957.

[126] H. Kim, D. Monllor-Satoca, W. Kim, W. Choi, *Energy Environ. Sci.* **2015**, *8*, 247-257.

[127] C. Wang, S. Yang, X. Chen, T. Wen, H. G. Yang, *J. Mater. Chem. A* **2017**, *5*, 910-913.

[128] W. Wang, W. Zhang, C. Hao, F. Wu, Y. Liang, H. Shi, J. Wang, T. Zhang, Y. Hua, *Sol. Energy Mater. Sol. Cells* **2016**, *152*, 1-9.

[129] C. W. Ahn, P. H. Borse, J. H. Kim, J. Y. Kim, J. S. Jang, C.-R. Cho, J.-H. Yoon, B. Lee, J.-S. Bae, H. G. Kim, J. S. Lee, *Appl. Catal. B: Environ.* **2018**, *224*, 804-809.

[130] F. Wang, Y. Liu, Z. Ma, H. Li, Z. Kang, M. Shen, *New J. Chem.* **2013**, *37*, 290-294.

[131] Z. Zhang, X. Li, C. Gao, F. Teng, Y. Wang, L. Chen, W. Han, Z. Zhang, E. Xie, *J. Mater. Chem. A* **2015**, *3*, 12769-12776.

[132] T. Nakajima, T. Nakamura, T. Tsuchiya, *Phys. Chem. Chem. Phys.* **2014**, *16*, 26901-26908.

[133] L. Ji, M. D. McDaniel, S. Wang, A. B. Posadas, X. Li, H. Huang, J. C. Lee, A. A. Demkov, A. J. Bard, J. G. Ekerdt, E. T. Yu, *Nat. Nanotechnol.* **2015**, *10*, 84-90.

[134] D. Sharma, S. Upadhyay, V. R. Satsangi, R. Shrivastav, U. V. Waghmare, S. Dass, *J. Phys. Chem. C* **2014**, *118*, 25320-25329.

[135] J. S. Jang, C. W. Ahn, S. S. Won, J. H. Kim, W. Choi, B.-S. Lee, J.-H. Yoon, H. G. Kim, J. S. Lee, *J. Phys. Chem. C* **2017**, *121*, 15063-15070.

[136] Q. Peng, J. Wang, Z. Feng, C. Du, Y. Wen, B. Shan, R. Chen, *J. Phys. Chem. C* **2017**, *121*, 12991-12998.

[137] D. Sharma, S. Upadhyay, V. R. Satsangi, R. Shrivastav, U. V. Waghmare, S. Dass, *Appl. Catal. B: Environ.* **2016**, *189*, 75-85.

[138] W. Yang, Y. Yu, M. B. Starr, X. Yin, Z. Li, A. Kvit, S. Wang, P. Zhao, X. Wang, *Nano Lett.* **2015**, *15*, 7574-7580.

[139] S. Park, S. Kim, H. J. Kim, C. W. Lee, H. J. Song, S. W. Seo, H. K. Park, D.-W. Kim, K. S. Hong, *J. Hazard. Mater.* **2014**, *275*, 10-18.

[140] W. Dong, B. Li, Y. Li, X. Wang, L. An, C. Li, B. Chen, G. Wang, Z. Shi, *J. Phys. Chem. C* **2011**, *115*, 3918-3925.

[141] Y. Wang, H. Xu, X. Wang, X. Zhang, H. Jia, L. Zhang, J. Qiu, *J. Phys. Chem. B* **2006**, *110*, 13835-13840.

[142] S. Venigalla, J. H. Adair, *Chem. Mater.* **1999**, *11,* 589-599.

[143] H. Tan, Z. Zhao, W. Zhu, E. N. Coker, B. Li, M. Zheng, W. Yu, H. Fan, Z. Sun, *ACS Appl. Mater. Interfaces* **2014**, *6*, 19184-19190.
[144] J. Hou, S. Cao, Y. Wu, F. Liang, L. Ye, Z. Lin, L. Sun, *Nano Energy* **2016**, *30*, 59-68.
[145] X. An, L. Zhang, B. Wen, Z. Gu, L.-M. Liu, J. Qu, H. Liu, *Nano Energy* **2017**, *35*, 290-298.
[146] S. Kumar, A. P. Singh, C. Bera, M. Thirumal, B. R. Mehta, A. K. Ganguli, *ChemSusChem* **2016**, *9*, 1850-1858.
[147] S. Kumar, R. Parthasarathy, A. P. Singh, B. Wickman, M. Thirumald, A. K. Ganguli, *Catal. Sci. Technol.* **2017**, *7*, 481-495.
[148] K. Kawashima, M. Hojamberdiev, O. Mabayoje, B. R. Wygant, K. Yubuta, C. B. Mullins, K. Domen, K. Teshima, *CrystEngComm* **2017**, *19*, 5532-5541.
[149] N. R. Manwar, R. G. Borkar, R. Khobragade, S. S. Rayalu, S. L. Jain, A. K. Bansiwal, N. K. Labhsetwar, *Int. J. Hydrogen Energy* **2017**, *42*, 10931-10942.
[150] M. Kodera, H. Urabe, M. Katayama, T. Hisatomi, T. Minegishi, K. Domen, *J. Mater. Chem. A* **2016**, *4*, 7658-7664.
[151] C. Zhang, Y. Li, M. Chu, N. Rong, P. Xiao, Y. Zhang, *RSC Adv.* **2016**, *6*, 24760-24767.
[152] S. J. A. Moniz, C. S. Blackman, P. Southern, P. M. Weaver, J. Tang, C. J. Carmalt, *Nanoscale* **2015**, *7*, 16343-16353.
[153] T. Minegishi, N. Nishimura, J. Kubota, K. Domen, *Chem. Sci.* **2013**, *4*, 1120-1124.
[154] S. Cho, J.-W. Jang, W. Zhang, A. Suwardi, H. Wang, D. Wang, J. L. MacManus-Driscoll, *Chem. Mater.* **2015**, *27*, 6635-6641.
[155] J. Feng, W. Luo, T. Fang, H. Lv, Z. Wang, J. Gao, W. Liu, T. Yu, Z. Li, Z. Zou, *Adv. Funct. Mater.* **2014**, *24*, 3535-3542.
[156] K. Maeda, K. Domen, *J. Phys. Chem. Lett.* **2010**, *1*, 2655-2661.
[157] S. Chen, Y. Qi, T. Hisatomi, Q. Ding, T. Asai, Z. Li, S. S. K. Ma, F. Zhang, K. Domen, C. Li, *Angew. Chem. Int. Ed.* **2015**, *54*, 8498-8501.
[158] C. Pan, T. Takata, M. Nakabayashi, T. Matsumoto, N. Shibata, Y. Ikuhara, K. Domen, *Angew. Chem. Int. Ed.* **2015**, *54*, 2955-2959.
[159] J. Seo, T. Hisatomi, M. Nakabayashi, N. Shibata, T. Minegishi, M. Katayama, K. Domen, *Adv. Energy Mater*. **2018**, *8*, 1800094.

REVIEW

Perovskite oxides are one of the most important classes of materials for the application as electrodes for photoelectrochemical (PEC) water splitting. Recent progress about the development of high-performance perovskite oxide-based electrodes for PEC water splitting is reviewed. The design strategies, challenges and perspectives of perovskite oxides as electrodes for PEC water splitting are also presented.

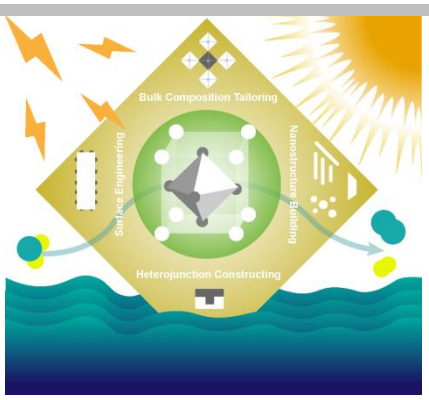

*Wei Wang[+], Meigui Xu[+], Xiaomin Xu, Wei Zhou, Zongping Shao**

Page No. 1 – Page No. 18

Perovskite Oxide-Based Electrodes for High-Performance Photoelectrochemical Water Splitting: A Review